Ultrafast Time-Resolved Carotenoid to-Bacteriochlorophyll Energy Transfer in LH2 Complexes from Photosynthetic Bacteria

Hong Cong,[‡] Dariusz M. Niedzwiedzki,[†] George N. Gibson,[‡] Amy M. LaFountain,[†] Rhiannon M. Kelsh,[†] Alastair T. Gardiner,[§] Richard J. Cogdell,[§] and Harry A. Frank*,[†]

Department of Chemistry, University of Connecticut, U-3060, 55 North Eagleville Road, Storrs, Connecticut 06269-3060, Department of Physics, University of Connecticut, U-3046, 2152 Hillside Road, Storrs, Connecticut 06269-3046, and Division of Biochemistry and Molecular Biology, Institute of Biomedical and Life Sciences, University of Glasgow, University Avenue, Glasgow, G12 8QQ, U.K.

Received: December 20, 2007; Revised Manuscript Received: May 1, 2008

Steady-state and ultrafast time-resolved optical spectroscopic investigations have been carried out at 293 and 10 K on LH2 pigment−protein complexes isolated from three different strains of photosynthetic bacteria: *Rhodobacter (Rb.) sphaeroides* G1C, *Rb. sphaeroides* 2.4.1 (anaerobically and aerobically grown), and *Rps. acidophila* 10050. The LH2 complexes obtained from these strains contain the carotenoids, neurosporene, spheroidene, spheroidenone, and rhodopin glucoside, respectively. These molecules have a systematically increasing number of π-electron conjugated carbon−carbon double bonds. Steady-state absorption and fluorescence excitation experiments have revealed that the total efficiency of energy transfer from the carotenoids to bacteriochlorophyll is independent of temperature and nearly constant at ∼90% for the LH2 complexes containing neurosporene, spheroidene, spheroidenone, but drops to ∼53% for the complex containing rhodopin glucoside. Ultrafast transient absorption spectra in the near-infrared (NIR) region of the purified carotenoids in solution have revealed the energies of the S_1 ($2^1A_g^-$) → S_2 ($1^1B_u^+$) excited-state transitions which, when subtracted from the energies of the S_0 ($1^1A_g^-$) → S_2 ($1^1B_u^+$) transitions determined by steady-state absorption measurements, give precise values for the positions of the S_1 ($2^1A_g^-$) states of the carotenoids. Global fitting of the ultrafast spectral and temporal data sets have revealed the dynamics of the pathways of de-excitation of the carotenoid excited states. The pathways include energy transfer to bacteriochlorophyll, population of the so-called S* state of the carotenoids, and formation of carotenoid radical cations ($Car^{\bullet+}$). The investigation has found that excitation energy transfer to bacteriochlorophyll is partitioned through the S_1 ($1^1A_g^-$), S_2 ($1^1B_u^+$), and S* states of the different carotenoids to varying degrees. This is understood through a consideration of the energies of the states and the spectral profiles of the molecules. A significant finding is that, due to the low S_1 ($2^1A_g^-$) energy of rhodopin glucoside, energy transfer from this state to the bacteriochlorophylls is significantly less probable compared to the other complexes. This work resolves a long-standing question regarding the cause of the precipitous drop in energy transfer efficiency when the extent of π-electron conjugation of the carotenoid is extended from ten to eleven conjugated carbon−carbon double bonds in LH2 complexes from purple photosynthetic bacteria.

Introduction

In photosynthetic bacteria, protein-bound carotenoids (Cars) harvest light from the sun and transfer the energy to nearby bacteriochlorophyll (BChl) molecules. This is highly advantageous to the organisms because Cars absorb light in the blue-green (450−550 nm) region of the visible spectrum where BChl does not, thereby supplementing the light-harvesting (LH) ability of BChl. However, the efficiency of Car-to-BChl energy transfer is not constant among LH pigment−protein complexes from different bacterial species. It varies from ∼90% in the light-harvesting 2 (LH2) complex from *Rhodobacter* (*Rb.*) *sphaeroides* 2.4.1, to ∼53% in the LH2 complex from *Rhodopseudomonas* (*Rps.*) *acidophila* strain 10050,[1,2] to ∼36% in the Car-reconstituted light-harvesting 1 (LH1) complex from *Rhodospirillum* (*Rsp.*) *rubrum*,[3] to as low as ∼20% in the LH1 complex from *Rps. acidophila*.[4] The reasons for the variability in efficiency are largely unknown, but are thought to depend on factors such as the nature, positions, and kinetics of the excited states of the Car, the orientation and distance of the Car with respect to the BChl, and the dynamics of the pathways for de-excitation of Car excited-state that compete with energy transfer to BChl.

Since the report of the structure of the LH2 complex from the purple bacterium, *Rps. acidophila*,[5] researchers have sought to correlate the structure with the pathways by which Cars transfer energy to BChl.[6–12] The structure of the LH2 complex from *Rps. acidophila* 10050 initially resolved to 2.5 Å,[5] and later to 2.0 Å,[13] consists of a circular array of nine heterodimer protein units (Figure 1), each consisting of a pair of α- and β-apoproteins that fold three BChls and one Car, rhodopin glucoside, into two concentric rings of transmembrane α-helices. The BChl molecules are arranged in two circular groups. One group has nine monomeric BChls and absorbs light at 800 nm (B800). Ten angstroms across the membrane, eighteen other more closely associated BChls absorb at 850 nm (B850). The

* Author to whom correspondence should be addressed. Fax: 860-486-6558. E-mail: harry.frank@uconn.edu.
‡ Department of Physics, University of Connecticut.
† Department of Chemistry, University of Connecticut.
§ University of Glasgow.

10.1021/jp711946w CCC: $40.75
Published on Web 07/31/2008

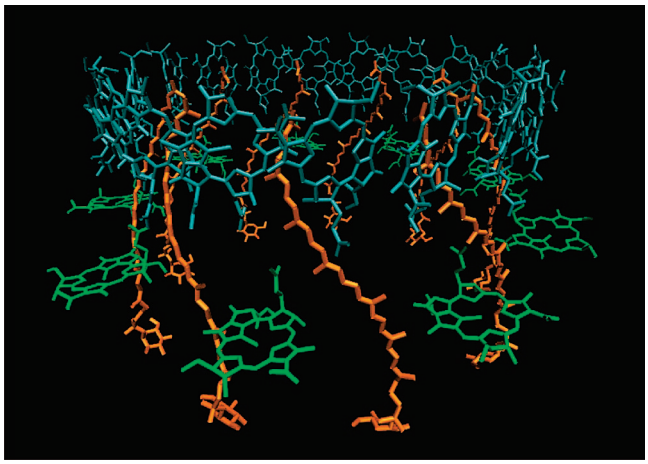

Figure 1. Structure of the LH2 antenna complex from *Rps. acidophila* 10050.

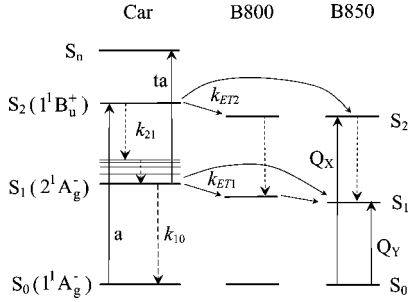

Figure 2. Simplified energy flow pathways of LH2 complexes from Car to BChl; a, absorption, ta, transient absorption. Dashed lines represent radiationless processes.

Cars span the width of the membrane and come within van der Waals distance of both B800 and B850 BChls.

In order to unravel the molecular factors controlling light-harvesting and to explain the variability in Car-to-BChl energy transfer efficiency it is important to understand the unique excited-state complexion of Cars. Unlike many π-electron conjugated organic molecules, direct excitation of Cars into the first excited singlet state, S_1 ($2^1A_g^-$), from the ground state, S_0 ($1^1A_g^-$), by one-photon absorption is forbidden by symmetry.[14–16] The major visible absorption and consequent strong coloration of Cars is due to absorption from S_0 ($1^1A_g^-$) into a higher excited singlet state, denoted S_2 ($1^1B_u^+$)[17–26] (see Figure 2). Both the S_1 ($2^1A_g^-$) and S_2 ($1^1B_u^+$) states act as energy donors to BChl and several investigations have reported the extent of partitioning of energy transfer efficiency between the two states.[8,10,27–32] Also, quantum theoretical computations on short polyenes, model systems for Cars, have revealed other exited states in the vicinity of S_1 ($2^1A_g^-$) and S_2 ($1^1B_u^+$).[33–35] Koyama et al. have suggested that a $1^1B_u^-$ state provides an alternate pathway to S_1 ($2^1A_g^-$) for internal conversion from S_2 ($1^1B_u^+$) and that it participates in energy transfer to BChl in the LH complexes.[36–40] However, this interpretation is controversial because it derives from theoretical computations on short polyenes[34,35] arbitrarily extrapolated to the longer carotenoids without consideration of environmental and substituent effects that may alter substantially the excited-state energies.[23] Also, there is no compelling indicator of excited-state symmetry in any of the spectroscopic observations. Recent femtosecond time-resolved stimulated Raman spectroscopic experiments on β-carotene by Mathies et al.[41,42] have reported that the dynamics of S_2 ($1^1B_u^+$) de-excitation are well explained without invoking an ultrafast-decaying intermediate state between S_2 ($1^1B_u^+$) and S_1 ($2^1A_g^-$).

Van Grondelle et al. investigated spirilloxanthin ($N = 13$) in solution and in LH1 pigment−protein complexes[43] and spheroidene ($N = 10$) and rhodopin glucoside ($N = 11$) in LH2 complexes[44] and suggested that an excited singlet state denoted S* participates in both the deactivation of these Cars and in the formation of Car triplet states in the LH complexes.[10] Other states with various nebulous designations, e.g., S_X[45] and $S^‡$,[46] have also been implicated in decay pathways following photoexcitation.[7–10,24,31,47,48] Recent experiments on various carotenes and xanthophylls have suggested that at least some of these state assignments may be due to twisted conformational forms of the molecules which would give rise to different spectroscopic features.[24,25]

Despite the detailed investigations described above, none have succeeded in explaining the highly variable Car-to-BChl energy transfer efficiency in the LH complexes. An important case in point is the precipitous drop from ~90 to ~53% in energy transfer efficiency reported for the LH2 complex from *Rps. acidophila* which contains rhodopin glucoside ($N = 11$) compared to the LH2 complex from *Rb. sphaeroides* 2.4.1 which contains spheroidene ($N = 10$). It has been suggested that the change is due to the S_1 ($2^1A_g^-$) energy of rhodopin glucoside being lower than the S_1 energy of BChl rendering the Car less able to transfer energy compared to spheroidene.[32] Indeed, the energy of the S_1 ($2^1A_g^-$) excited-state of the Car relative to that of the bound BChls is an important factor that can affect the efficiency of Car-to-BChl energy transfer. However, due to the forbidden nature of the S_0 ($1^1A_g^-$) ↔ S_1 ($2^1A_g^-$) transitions, the S_1 ($2^1A_g^-$) state energy values are not easily obtained, and there are discrepancies in the values reported by various spectroscopic methods.[9] Reports of S_1 ($2^1A_g^-$) energies using fluorescence spectroscopy[49–54] have yielded values up to ~800 cm^{-1} higher than those based on S_1 ($2^1A_g^-$) → S_2 ($1^1B_u^+$) transient absorption experiments.[6,30,52,55–58] Table 1 gives the values of the S_1 ($2^1A_g^-$) energies of the Cars, neurosporene ($N = 9$), spheroidene ($N = 10$), spheroidenone ($N = 10+$, where the + indicates a carbonyl group in conjugation with the π-electron carbon−carbon double bond chain), and rhodopin glucoside ($N = 11$) from fluorescence and transient absorption studies in solution and in LH2 complexes. The reason for the discrepancy in the values obtained by the different approaches has been suggested to be due to fluorescence and transient absorption probing different conformational geometries of the Car in the S_1 ($2^1A_g^-$) state.[6]

This paper presents a steady-state and ultrafast time-resolved spectroscopic investigation at room and cryogenic temperatures of four different LH2 pigment−protein complexes containing the Cars, neurosporene, spheroidene, spheroidenone, or rhodopin glucoside (Figure 3). Steady-state absorption and fluorescence excitation experiments have revealed the total efficiency of energy transfer to BChl. Transient absorption spectra of the purified Cars in solution in the near-infrared (NIR) region have systematically probed their S_1 ($2^1A_g^-$) → S_2 ($1^1B_u^+$) transitions and yielded precise values for the S_1 ($2^1A_g^-$) energies of the molecules. Global fitting of the ultrafast spectral and temporal data sets from experiments done at both room and low temperatures have revealed the pathways for de-excitation of the Car excited states which involve not only energy transfer to BChl, but also Car radical cation ($Car^{•+}$) formation previously unreported for the LH2 complexes containing spheroidenone and rhodopin glucoside.[6,8] The goal of this investigation is to

TABLE 1: Energies of the S_2 ($1^1B_u^+$) and S_1 ($2^1A_g^-$) States of Carotenoids and the Q_X and Q_Y Transitions of Bacteriochlorophylls[a]

			S_1 (cm^{-1})				
carotenoid	*N*	S_2 (cm^{-1})	fluorescence	$S_1 \rightarrow S_2$[b]	system	T (K)	ref[c]
neurosporene	9	20 780		14 170 ± 50	acetone	293	
		20 240			LH2	10	
		20 330			LH2	293	
		21 300	15 300		*n*-hexane	293, 170	49
spheroidene	10	20 010		13 160 ± 50	acetone	293	
		19 420			LH2	10	
		19 570			LH2	293	
			14 200		*n*-hexane	293, 200	49
		19 530		13 400 ± 100	LH2	293	6
		20 700		13 400 ± 90	*n*-hexane	293, 186	6, 56
spheroidenone	10+	19 460		12 800 ± 50	*n*-hexane	293	
		18 070			LH2	10	
		17 790			LH2	293	
		19 500		13 000 ± 100	*n*-hexane	293	64
rhodopin glucoside	11	19 760		12 400 ± 50	acetone	293	
		18 900			LH2	10	
		19 080			LH2	293	
		19 050		12 550 ± 200	LH2	293	6
		20 000		12 800 ± 150	methanol	293	6
bacteriochlorophyll		Q_X (cm^{-1})	Q_Y (cm^{-1})				
BChl *a*		16 490	12 950		methanol	293	84
LH2 B800		17 040	12 520		G1C	10	
		16 950	12 520		G1C	293	
		17 010	12 530		2.4.1 anaerobic	10	
		16 950	12 520		2.4.1 anaerobic	293	
		17 090	12 520		2.4.1 aerobic	10	
		17 010	12 480		2.4.1 aerobic	293	
		16 920	12 470		10050	10	
		16 920	12 480		10050	293	
LH2 B850		17 040	11 710		G1C	10	
		16 950	11 810		G1C	293	
		17 010	11 740		2.4.1 anaerobic	10	
		16 950	11 790		2.4.1 anaerobic	293	
		17 090	11 740		2.4.1 aerobic	10	
		17 010	11 790		2.4.1 aerobic	293	
		16 920	11 510		10050	10	
		16 920	11 680		10050	293	

[a] The energies of the S_2 ($1^1B_u^+$) state of Cars have an uncertainty of 40 cm^{-1}, the energies of the Q_X and Q_Y transitions of BChl *a* in methanol have an uncertainty of 30 cm^{-1}, and the energies of the B800 and B850 Q_Y transitions an uncertainty of 20 cm^{-1}, which are based on the 1 nm spectral resolution of the steady state absorption spectrometer. [b] The S_1 ($2^1A_g^-$) energies were obtained from NIR transient absorption measurements of the S_1 ($2^1A_g^-$) → S_2 ($1^1B_u^+$) transition energies subtracted from the S_0 ($1^1A_g^-$) → S_2 ($1^1B_u^+$) transition energies. [c] No reference means this work.

understand the molecular factors controlling the rates and efficiencies of Car-to-BChl energy transfer in this important class of photosynthetic pigment−protein complexes.

Materials and Methods

Culture Growth. *Rb. sphaeroides* strains 2.4.1 and G1C were grown in peptone yeast extract medium (ATCC No. 526), and *Rps. acidophila* 10050 was grown in *Rps.* medium (ATCC No. 650) anaerobically in 1 and 2 L bottles at 30 °C under continuous illumination using three 60 W incandescent bulbs. *Rb. sphaeroides* 2.4.1 was also grown aerobically to produce cells having a high content of spheroidenone. The cells were harvested by centrifugation at 12 000 g for 10 min at 4 °C using an SS-34 rotor in a Sorvall RC-5B centrifuge. The preparations of pigment−protein complexes were performed in low light with samples being maintained on ice unless otherwise noted.

Preparation of Chromatophores. Whole packed cells were diluted with 15 mM Tris buffer, pH 8.0, to obtain an optical density at the maximum absorption band near 860 nm (OD_{860}) of approximately 50 in a 1 cm path length cuvette. The suspension was then subjected to French pressure cell press (SLM Aminco) disruption at 20 000 psi to rupture the cells, and the resulting solution was centrifuged at 12 000 g for 10 min at 4 °C to remove unbroken cells and other cellular debris. The supernatant containing the chromatophores was then ultracentrifuged at 180 000 g for 60 min at 4 °C using a Beckman L8−55 M Ultracentrifuge.

LH2 Isolation. The pellet from the ultracentrifugation procedure was resuspended in approximately five times its volume of 15 mM Tris buffer pH 8.0 containing 150 mM NaCl and adjusted to an OD_{860} of 50. Thirty percent LDAO was added dropwise while stirring to a final concentration of 0.6% v/v. The sample was then left to incubate at 293 K in the dark for 30 min. Following the incubation period, the sample was again ultracentrifuged for 60 min at 180 000 g at 4 °C. The supernatant exhibited an absorption spectrum of reaction centers and was saved for use in other experiments. Pelleted material was taken up in 15 mM Tris pH 8.0, 150 mM NaCl, and 0.6% LDAO, incubated for 30 min, and centrifuged at 180 000 g for 60 min at 4 °C. This process was repeated until the absorption spectrum

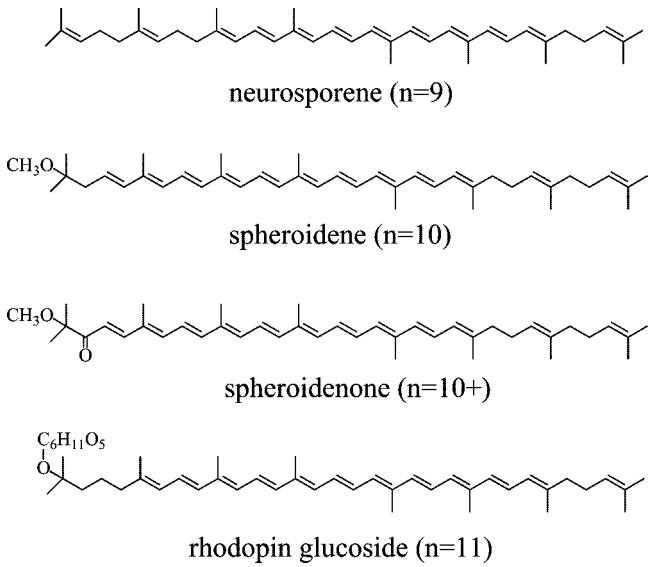

Figure 3. Structures of the all-*trans* isomers of neurosporene, spheroidene, spheroidenone, and rhodopin glucoside.

of the supernatant displayed that of LH2. The LH2 sample was then dialyzed overnight against 15 mM Tris buffer pH 8.0, 0.06% LDAO and purified using column chromatography.

Purification of LH2 Complexes and Carotenoids. The isolated LH2 complexes were loaded onto a 2.5 cm diameter × 28 cm height column containing 40 mL of DEAE Sephacel (Sigma-Aldrich). Prior to loading, the column was equilibrated with approximately 5 bed volumes of 15 mM Tris buffer pH 8.0 and 0.06% LDAO. After loading, the column was washed with the equilibrating buffer until the eluate ran clear. This process removed the free pigments. A series of solutions containing increasing NaCl concentration (80, 100, 125, 150, 180, 200, 250 mM NaCl) were then added to the column. The column was washed with each solution until the eluate ran clear. This required from 250−500 mL of each solution. Reaction centers eluted from the column at 180 mM NaCl and appeared pale yellow. LH2 followed directly after at 200 mM NaCl and appeared bright green. Repetition of this column procedure was occasionally necessary to achieve a high level of purity based on the appearance of the absorption spectrum. Samples were concentrated using a Centriplus YM-10 Amicon concentrator and dialyzed overnight in a dark 4 °C cold room against 15 mM Tris pH 8.0, 0.06% LDAO. The carotenoid composition of the LH2 complexes was analyzed by HPLC after extracting the pigments as previously described.[25] It was determined that the LH2 complexes from *Rb. sphaeroides* G1C, 2.4.1 (anaerobic), 2.4.1 (aerobic), and *Rps. acidophila* 10050 contained 99% neurosporene, 99% spheroidene, 93% spheroidenone, and 93% rhodopin glucoside, respectively. The carotenoid fractions from the HPLC were collected and, along with the purified LH2 complexes, were stored in the dark at −80 °C until ready for use in the spectroscopic experiments.

Spectroscopy. Purified LH2 complexes were dissolved in an aqueous buffer containing 15 mM Tris, 0.06% LDAO at pH 8.0. Steady-state absorption spectroscopy was carried out using a Varian Cary 50 spectrometer. Fluorescence and fluorescence excitation spectroscopy was performed using a Jobin-Yvon Fluorolog 3 spectrometer equipped with a Hamamatsu R928P photomultiplier. The emission from the samples was monitored using right-angle detection with excitation and emission slit widths of 3 mm (band-pass of 6 nm) and 5 mm (band-pass of 10 nm), respectively. The fluorescence excitation spectra of LH2 complexes were detected at the maximum of BChl emission bands near 860 nm using the same excitation and emission slit widths as for emission. All fluorescence spectra were corrected for the excitation lamp profile and response profile of the detector. For the ultrafast optical experiments at 293 K, the optical density (OD) of the samples was adjusted to ∼0.4 at the maximum of the (0−0) spectral origin of the Car S_0 ($1^1A_g^-$) → S_2 ($1^1B_u^+$) transition in a 2 mm path length quartz cuvette. For the experiments at 10 K, the OD was ∼0.4 in a 4 mm path length plastic cuvette after mixing with glycerol to a final concentration of 60% v/v. A Janis, model STVP-100−1 helium cryostat was used for all the experiments performed at 10 K.

The details of the femtosecond transient absorption spectrometer have been previously described.[59,60] Briefly, the system is based on an amplified Ti:Sapphire laser system (Spectra-Physics) operating at 1 kHz repetition rate. Pump pulses were obtained from an optical parametric amplifier (Spectra-Physics) with a pulse duration of ∼100 fs, and the probe laser pulses were derived from a white light continuum (450−750 nm in the visible region and 750−1350 nm in the NIR) generated by a nonlinear crystal (Ultrafast Systems LLC).The pump and probe were overlapped at the sample at the magic-angle (54.7°) polarization. The energy of the pump pulse was 1 μJ which corresponded to a photon density of 3×10^{14} photons cm^{-2} for a spot size of the pump pulse of 1.2 mm in diameter.

An instantaneous bleach signal was used to determine the zero time-delay. A polarizer was placed in front of the spectrometer to minimize the scattered signal from the pump beam, and the signals were averaged over 5 s. For detection in the visible spectral region, a spectrometer equipped with a charge-coupled detector was used (Ocean Optics). In the NIR region, a superconducting single-photon detector was used (Sensors Unlimited).

For the 293 K experiments, the sample was mixed continuously using a magnetic microstirrer to prevent photodegradation. The integrity of the samples was confirmed by steady-state absorption spectroscopy before and after every transient absorption experiment. All transient absorption experiments were done by exciting the (0−0) spectral origin of the Cars with the pump beam. Surface Explorer (v.1.0.6) (Ultrafast Systems LCC) was used to correct for dispersion in the transient absorption spectra and also to determine the principle number of the kinetic components by singular value decomposition. ASUFit 3.0 software provided by Dr. Evaldas Katilius at Arizona State University with local modifications was used for global fitting analysis. The quality of the fitting was evaluated based on the minimization of the residual parameter chi square (χ^2).

Results

Steady-State Absorption Spectra. The steady-state absorption spectra of LH2 complexes from *Rb. sphaeroides* G1C, *Rb. sphaeroides* 2.4.1 (anaerobic), *Rb. sphaeroides* 2.4.1 (aerobic), and *Rps. acidophila* 10050 in buffer (15 mM Tris, 0.06% LDAO, pH = 8.0) at 293 K and in buffer/glycerol (v/v, 40/60) at 10 K are shown in Figure 4. The vibronic resolution of the steady-state absorption spectra taken at 10 K (dark solid lines in Figure 4) in buffer/glycerol is enhanced significantly compared to the 293 K spectra (light solid lines in Figure 4). Low temperatures tend to narrow the spectral features of Cars and BChls.[21,61,62] All of the spectra show the characteristic vibronic profile of the S_0 ($1^1A_g^-$) → S_2 ($1^1B_u^+$) transition of the Cars in the 400−550 nm region. The lower vibrational resolution of spheroidenone compared to other Cars is due to increased conformational disorder brought about by the presence of a

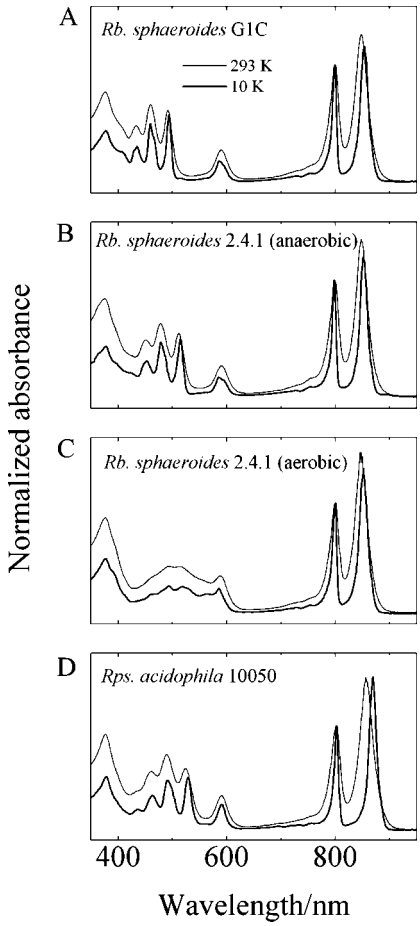

Figure 4. Steady-state absorption spectra of LH2 complexes from (A) *Rb. sphaeroides* G1C, (B) *Rb. sphaeroides* 2.4.1 (anaerobic), (C) *Rb. sphaeroides* 2.4.1 (aerobic), and (D) *Rps. acidophila* 10050 in a buffer at 293 K and in buffer/glycerol (40/60, v/v) at 10 K. The spectra were normalized to their absorption bands at 800 nm.

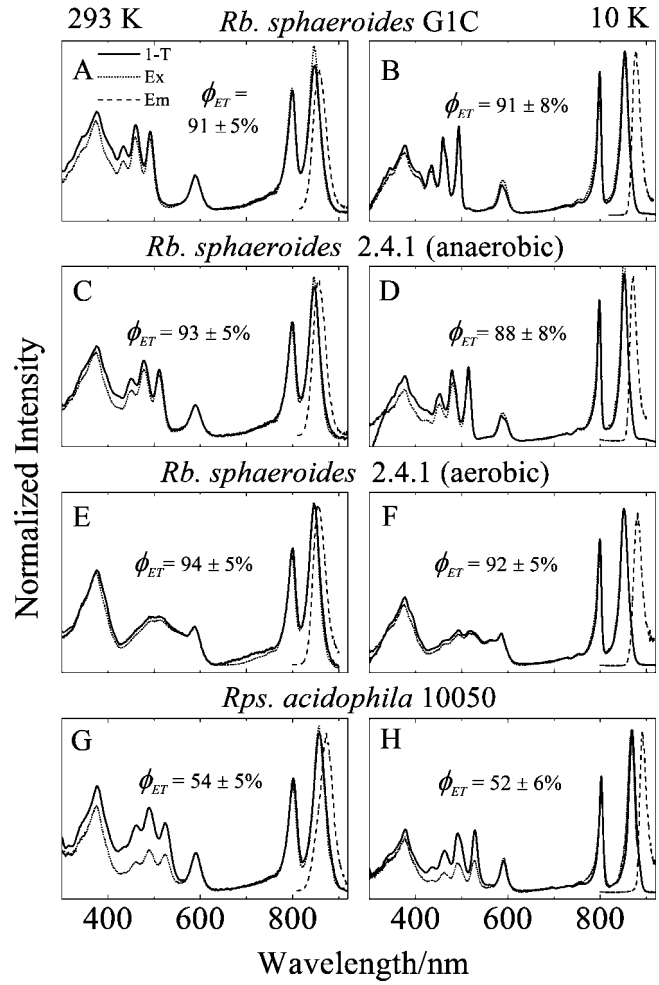

Figure 5. Emission (Em), fluorescence excitation (Ex), and 1-T (where T is transmittance) spectra of the LH2 complexes in buffer at 293 K, and in buffer/glycerol at 10 K. The emission spectra were detected at 856 nm in (A), (C), and (E), at 877 nm in (B), at 870 nm in (D), at 880 nm in (F), at 872 nm in (G), and at 891 nm in (H).

carbonyl group in the π-electron conjugation (Figure 3).[63,64] The peak positions shift to longer wavelength as the conjugation length increases, as expected from simple quantum mechanical models of π-electron conjugated systems.[23,34,65] As the temperature is lowered from 293 to 10 K, the peak positions of the Cars shift 2−5 nm to longer wavelength due to the increase in the index of refraction of the sample. Also, upon lowering the temperature the Franck−Condon maximum of the Car absorption changes from the (0−1) vibronic band to the (0−0) band, and in the spectra of the LH2 complexes from *Rb. sphaeroides* G1C and 2.4.1 (anaerobic), the BChl Q_x band at 590 nm is split into two bands. This is not observed in the spectra from the LH2 complexes of *Rb. sphaeroides* (aerobic) 2.4.1 and *Rps. acidophila* suggesting that the structures may be slightly different.

The LH2 absorption spectra also show features attributed to the BChls. For all complexes, the shapes and positions of the Soret, Q_X, and Q_Y B800 and B850 bands are very similar.[8,66] At 293 K, the B850 peak position for the LH2 complexes from *Rb. sphaeroides* G1C, *Rb. sphaeroides* 2.4.1 (anaerobic), and *Rb. sphaeroides* 2.4.1 (aerobic) is 848 ± 1 nm, and shifts to 853 ± 1 nm at 10 K. For the LH2 complex from *Rps. acidophila* 10050, the B850 band at 293 K appears at 856 ± 1 nm and shifts to 869 ± 1 nm at 10 K.

Energy Transfer Efficiency. Emission spectra (dashed lines in Figure 5) were recorded for each sample to determine the optimal detection wavelength for the fluorescence excitation measurements. The Car-to-BChl excitation energy transfer (EET) efficiencies were determined by comparing the amplitudes of the Car peaks in the fluorescence excitation spectra (dotted lines in Figure 5) with those in the absorption spectra expressed as 1-T, where T is the transmittance (solid lines in Figure 5).[67] At 293 K, the Car-to-BChl EET efficiencies were found to be 91 ± 5, 93 ± 5, 94 ± 5, and 54 ± 5%, for the LH2 complexes from *Rb. sphaeroides* G1C, *Rb. sphaeroides* 2.4.1 (anaerobic), *Rb. sphaeroides* 2.4.1 (aerobic), and *Rps. acidophila* 10050, respectively. At 10 K the values were 91 ± 8, 88 ± 8, 92 ± 5, and 52 ± 6%. This is consistent with a previous report that Car-to-BChl EET efficiency is not affected by temperature.[68] Note that the EET efficiencies for the LH2 complexes having Cars with N = 9, 10, and 10+ are similar (∼90%) and significantly higher than the EET efficiency of ∼53% for the LH2 complex from *Rps. acidophila* 10050 (N = 11).

Transient Absorption in the Visible Spectral Region. Transient absorption spectra of the LH2 complex from *Rb. sphaeroides* G1C in the region 450−750 nm taken at 293 and 10 K at various delay times after the Car excitation laser pulse are shown in Figure 6A,C. Upon excitation at either temperature, there is an immediate onset of a bleaching of the strongly allowed S_0 ($1^1A_g^-$) → S_2 ($1^1B_u^+$) absorption in the region 450−500 nm (black lines in Figure 6A,C). In addition, bleaching of the BChl Q_X band at 590 nm is observed, indicating ultrafast

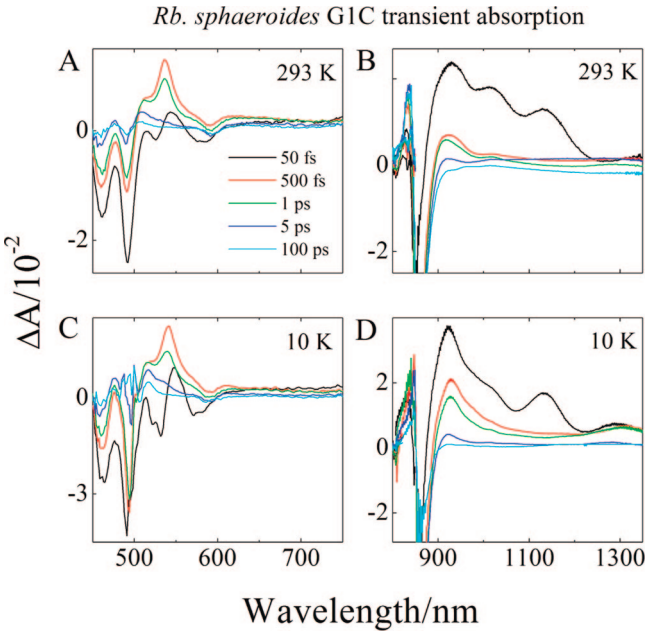

Figure 6. Transient absorption spectra of LH2 from *Rb. sphaeroides* G1C at 293 and 10 K.

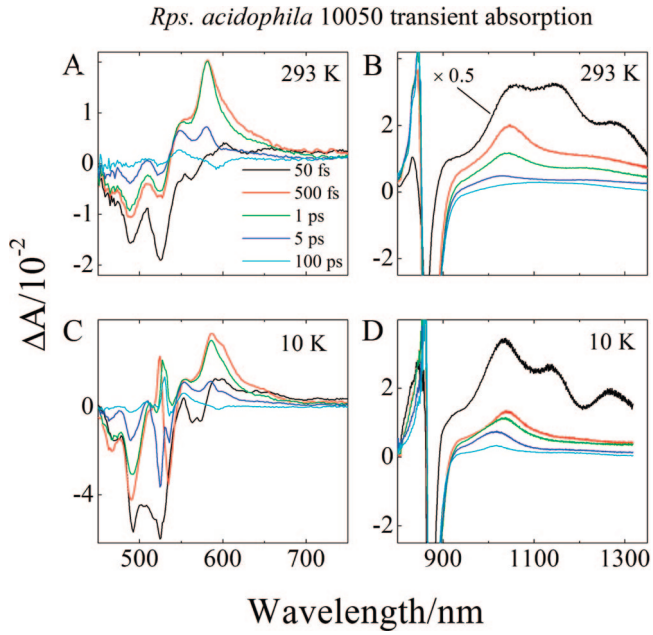

Figure 7. Transient absorption spectra of LH2 from *Rps. acidophila* 10050 at 293 and 10 K.

EET from the Car S_2 ($1^1B_u^+$) state to BChl. At 500 fs (red lines in Figure 6A,C), the Car bleaching partially recovers, but the Q_X bleaching persists. Also, at this time the positive band at ~550 nm gives way to a strong transient absorption signal that peaks at ~540 nm.This latter signal is the well-known S_1 ($2^1A_g^-$) → S_n transition of the Car.[8,25] As time evolves to 1 ps (green lines in Figure 6A,C) the S_1 ($2^1A_g^-$) → S_n transient absorption peak is reduced in intensity due to EET from the S_1 ($2^1A_g^-$) of the Car to BChl. Because the lifetime of the S_1 ($2^1A_g^-$) state of purified neurosporene in solution is known to be ~25 ps,[25] the fact that the reduction in intensity of the S_1 ($2^1A_g^-$) → S_n transient absorption occurs in ~1 ps suggests that EET from the S_1 ($2^1A_g^-$) state is highly efficient. Also, a pronounced shoulder at ~510 nm on the short wavelength side of the S_1 ($2^1A_g^-$) → S_n transition is evident in the 500 fs (red lines in Figure 6A,C) trace and even more noticeable at 1 ps (green lines in Figure 6A,C). At 5 ps (dark blue lines in Figure 6A,C), the shoulder persists while the S_1 ($2^1A_g^-$) → S_n transition intensity has almost completely disappeared. This shoulder is the characteristic signal of the Car S* state, which has been proposed to be a conformationally twisted form of the Car molecule in S_1 ($2^1A_g^-$).[24,25] In the 100 ps traces (cyan lines in Figure 6A,C), the Q_X bleaching remains, and there also appears excited-state absorption (ESA) at ~507 nm at 293 K and at ~517 nm at 10 K that persists for a much longer time. This long-lived ESA is attributable to the formation of a Car triplet state.[43]

Transient absorption spectra of the LH2 complexes from *Rb. sphaeroides* 2.4.1 (anaerobic), *Rb. sphaeroides* 2.4.1 (aerobic), and *Rps. acidophila* 10050 taken at 293 and 10 K (Supporting Information, Figures S1A,C and S2A,C, and Figure 7A,C) show very similar spectral behavior to the LH2 complex from *Rb. sphaeroides* G1C with two notable differences: (1) The peak positions for the Car bleaching and the S_1 ($2^1A_g^-$) → S_n transient absorption are red-shifted as the π-electron conjugation length of the Car becomes longer; (2) The 500 fs spectra from the LH2 complex from *Rps. acidophila* 10050 (red lines in Figure 7A,C) are very broad, having absorption intensity stretching out beyond 650 nm, compared to the spectra in this time domain from the other LH2 complexes, and also relative to the spectra taken at 1 ps from this LH2 complex (green lines in Figures 7A,C). This is attributable to a transition from a vibronically hot S_1 ($2^1A_g^-$) state to a higher excited singlet. The transition is red-shifted relative to the S_1 ($2^1A_g^-$) → S_n transition and relaxes on the time scale of hundreds of femtoseconds.[10,24,25,31,46–48,60,69] Slight evidence for this is present in the spectra from the other LH2 complexes. Broad positive absorption appears around 570 nm in the 500 fs trace of the LH2 complex from *Rb. sphaeroides* 2.4.1 (anaerobic) taken at 10 K (red line in Supporting Information, Figure S1C) and between 600 and 700 nm in the 500 fs trace of the LH2 complex from *Rb. sphaeroides* 2.4.1 (aerobic) taken at 10 K (red line in Supporting Information, Figure S2C). However, only in the LH2 complex from *Rps. acidophila* 10050 is this broadening so clearly seen, and it is substantially diminished as time progresses to 1 ps.

Experiments by Herek et al.[70,71] have reported carotenoid spectral band shifts upon direct photoexcitation of BChl in LH2 complexes. These bandshifts were attributed to a Stark effect induced by changes in the local electric field near the carotenoid molecules. In experiments on LH2 complexes from *Rps. acidophila*, the bandshifts were reported to decay with lifetime of 1.5 ps.[71] We observed no such kinetic component in our analysis of either room temperature or 10 K visible data sets where these signals might appear. However, direct carotenoid excitation is used in the present experiments, and because this gives rise to strong ground-state bleaching signals, manifestations of carotenoid bandshifts would undoubtedly be masked.

Transient Absorption in the NIR Spectral Region. Transient absorption spectra of the LH2 complex from *Rb. sphaeroides* G1C in the NIR region taken at different delay times at 293 and 10 K are shown in Figure 6B,D. The spectra in this region are dominated by a very strong negative band (bleaching) near 850 nm associated with excited B850. This bleaching sets in within the time course of the pump laser pulse and persists for hundreds of picoseconds. The rapid onset is strong evidence for transfer from the initially excited S_2 ($1^1B_u^+$) state of the Car to the BChl B850. The spectrum taken at 50 fs at 293 K (black line in Figure 6B) has three major positive peaks at 929, 1015, and 1130 nm. The transient absorption spectrum taken at

50 fs at 10 K (black line in Figure 6D) has absorption bands at similar positions: 923, 1010, and 1130 nm, plus an additional peak at 1310 nm which is hardly noticeable in the 293 K spectrum. In the 10 K spectrum, the peak at 1010 nm is less resolved than the corresponding peak at 1015 nm in the 293 K spectrum. Because the signals at 1015 nm (293 K) and 1010 nm (10 K) and 1130 nm (both temperatures) disappear in less than a few hundred femtoseconds (Figure 6B,D) they are attributed to an S_2 ($1^1B_u^+$) → S_n transition. This assignment is supported by an ultrafast transient absorption spectrum of neurosporene in EPA (diethyl ether/isopentane/ethanol, 5/5/2, v/v/v) at 77 K which shows very similar peaks and kinetic behavior.[72]

The transient absorption spectrum of the LH2 complex from *Rb. sphaeroides* G1C taken at 1 ps (green line in Figure 6B) at 293 K shows a strong absorption band at 920 nm, and a smaller peak at 1020 nm. At 10 K, the peak at 920 nm sharpens (green line in Figure 6D). These signals have been attributed to $Car^{\bullet+}$ formation in the LH2 complex[6,8] due to their similarity to the D_0 → D_2 doublet transition of $Car^{\bullet+}$ in solution.[73–75] A weak signal observed at ∼1300 nm may be attributed to D_0 → D_1 transient absorption as was previously assigned in the NIR spectrum of the LH2 complex obtained from *Rb. sphaeroides* G1C.[8]

In going from a delay time of 500 fs to 1 ps the band at 920 nm sharpens, consistent with vibronic cooling, analogous to that seen for the S_1 ($2^1A_g^-$) state in the visible region. The wavelength region between 900 and 1600 nm also contains signals associated with an S_1 ($2^1A_g^-$) → S_2 ($1^1B_u^+$) electronic transition.[55,72] For neurosporene in an EPA glass at 77 K, this signal decays in ∼25 ps consistent with the S_1 ($2^1A_g^-$) lifetime of the molecule.[70] In the LH2 complex of *Rb. sphaeroides* G1C the signal decays much faster (on the order of 1 ps) due to EET from the S_1 ($2^1A_g^-$) state of the Car to BChl.

The transient absorption spectra of the LH2 complexes from *Rb. sphaeroides* 2.4.1 (anaerobic), *Rb. sphaeroides* 2.4.1 (aerobic), and *Rps. acidophila* 10050 taken at 293 and 10 K are shown in Figures S1B and D, S2B and D, and 7B and D, respectively. All of these show very similar spectral behavior to the LH2 complex from *Rb. sphaeroides* G1C LH2, but there are two notable differences: (1) The transient absorption spectra taken at 293 and 10 K at a 50 fs time delay for *Rb. sphaeroides* 2.4.1 (aerobic) (black lines Figures S2B and D) are very broad and featureless. This is undoubtedly due to the increased conformational disorder of spheroidenone as described above for its steady-state absorption spectrum; (2) Most of the NIR absorption bands shift with increasing conjugation length of the Car. This includes the bands associated with the S_2 ($1^1B_u^+$) → S_n transition and the $Car^{\bullet+}$, both of which shift to longer wavelength, and the S_1 ($2^1A_g^-$) → S_2 ($1^1B_u^+$) transition which shifts to shorter wavelength. For example, in the 1 ps transient absorption spectrum taken at 10 K from the LH2 from *Rb. sphaeroides* G1C (green line in Figure 6D), the $Car^{\bullet+}$ band appears at 920 nm. This same band appears at 961 nm for the LH2 complex from *Rb. sphaeroides* 2.4.1 (anaerobic) (green line in Supporting Information, Figure S1D), and at 1041 nm for the LH2 complex from *Rps. acidophila* 10050 (green line in Figure 7D). For the LH2 complex from *Rb. sphaeroides* 2.4.1 (aerobic) containing spheroidenone, the band appears at 960 nm (green line in Supporting Information, Figure S2D). A previous investigation[8] failed to observe a $Car^{\bullet+}$ signal from the LH2 complex from *Rb. sphaeroides* 2.4.1 (aerobic) containing spheroidenone because the 293 K NIR spectrum was taken at a time delay fixed at 1 ps. At this time delay and temperature

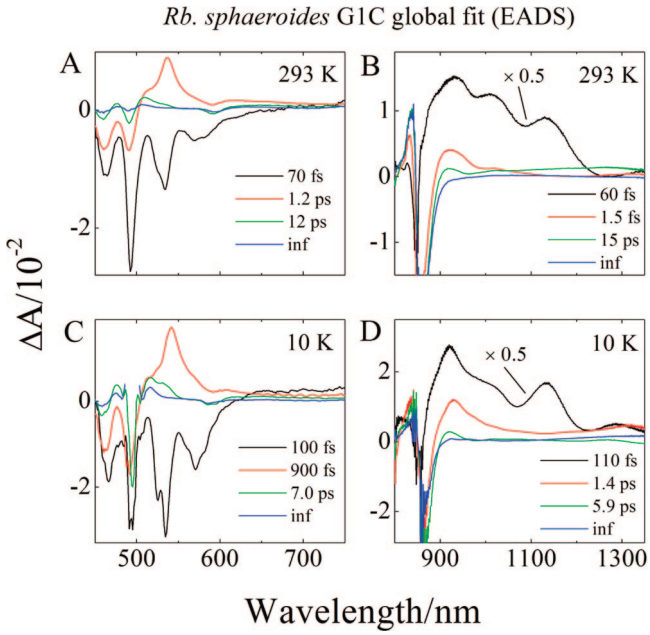

Figure 8. Evolution associated difference spectra (EADS) of LH2 from *Rb. sphaeroides* G1C.

the signal has already substantially decayed and possesses only very small amplitude (see the green line in Supporting Information, Figure S2B). Another very small broad signal is observed at 1017 nm (e.g., see the red and green traces in the spectra for the LH2 complex from *Rb. sphaeroides* G1C in Figure 6B and Supporting Information, Figure S3). Because this signal does not change wavelength depending on the complex, and based on spectroscopic studies of BChl *a* in solution and in other pigment−protein complexes, it has been assigned to the transient absorption maximum of a BChl *a* anion formed in conjunction with the $Car^{\bullet+}$.[8,76,77]

In order to obtain a more thorough understanding of the dynamics of the pathways for de-excitation of photoexcited Cars and EET to BChl, global fitting of the spectral and temporal data sets were undertaken.

Global Analysis in the Visible Spectral Region. The results of a global fitting analysis of the 293 and 10 K data sets obtained in the visible spectral region from the LH2 complex from *Rb. sphaeroides* G1C using a sequential decay model[24,78] are shown in Figure 8A,C. The fitting results are referred to as evolution associated difference spectra (EADS) and reveal the evolution of the difference spectra as time elapses. An EADS analysis is extremely useful in deducing effective lifetimes of excited states. These lifetimes will correspond to actual decay times for any part of the overall pathway that involves sequential steps. Four EADS components were needed to obtain a satisfactory fit based on the minimization of χ^2. The components display very similar amplitude spectra at 293 and 10 K (compare Figures 8A and C). The initial EADS component (black lines in Figures 8A and C) is comprised of a series of strong negative bands in the region 440 to 630 nm corresponding to the bleaching of the strongly allowed S_0 ($1^1A_g^-$) → S_2 ($1^1B_u^+$) absorption as well as stimulated emission from S_2 ($1^1B_u^+$). The component has a 70 fs decay time for the 293 K data set and a 100 fs decay time for the 10 K data set. These are associated with the decay of the Car S_2 ($1^1B_u^+$) state.[24,36,60] The second EADS component (red lines in Figure 8A,C) displays weaker negative bands in the 450 to 500 nm region than the first EADS, a strong positive band in the region 500 to 590 nm due to the S_1 ($2^1A_g^-$) → S_n absorption transition, and also a pronounced dip at 590 nm due

to the bleaching of the Q_X band of the BChl. The smaller amplitude of the negative bands in the 450 to 500 nm region in the second EADS compared to those in the first EADS indicate that the ground-state absorption bleaching has recovered to some degree in this time domain. The lifetime of the second component is 1.2 ps at 293 K and 900 fs at 10 K and is assigned to the S_1 ($2^1A_g^-$) lifetime of neurosporene in the LH2 complex.[25,37,38,60] As the second EADS component evolves to a third (green lines in Figure 8A,C), most of the amplitude associated with the S_1 ($2^1A_g^-$) → S_n absorption transition has disappeared, but there remains a clearly positive band at 530 nm in the data sets taken at both temperatures. In addition wavy features reminiscent of spectral band shifts are evident in the region of the Car ground-state absorption between 450 and 525 nm (e.g., see the green line in Figure 8A). This EADS component has a 12 ps lifetime at 293 K and a 7.0 ps lifetime at 10 K and corresponds well with the previously reported lifetime of the S* state.[7,8,10,31,44] The fourth EADS (dark blue lines in Figure 8A,C) have infinitely long lifetimes on the time scale of the experiment, and possess similar, albeit lower amplitude peaks as the third EADS in the region of the ground-state bleaching. This component is associated with the triplet state of neurosporene thought to be formed from the S* state as well as bleaching of the BChl Q_X band which lasts for nanoseconds.[7,8,10,31,44] The lower amplitude of the fourth EADS in the region of the ground-state bleaching compared to the third EADS indicates a return of some of the population to the ground-state during this time interval.

The global fitting obtained from the 293 and 10 K data sets from the LH2 complexes from *Rb. sphaeroides* 2.4.1 (anaerobic), *Rb. sphaeroides* 2.4.1 (aerobic), and *Rps. acidophila* 10050 in the visible spectral region are shown in Supporting Information, Figures S4A,C and S5A,C, and Figures 9A,C. All display similar amplitude spectra as seen for the global fits to the data sets from the LH2 complex from *Rb. sphaeroides* G1C (Figure 8A,C), but there are a couple of differences: (1) As expected for the different complexes, the peak positions for the Car bleaching and transient absorption are red-shifted with increasing π-electron conjugation length of the Car; (2) For all the data sets except that from the LH2 complex from *Rps. acidophila* 10050, four kinetic components were required for an acceptable fit. In the case of the LH2 complex from *Rps. acidophila* 10050, an additional EADS component having a lifetime of 320 fs (293 K) and 350 fs (10 K) (magenta lines in Figure 9A,C) was necessary to obtain a good fit. This additional component exhibits a broad EADS line shape red-shifted compared to the third EADS which is clearly assigned to the well-characterized S_1 ($2^1A_g^-$) → S_n transition. This indicates that the additional component is associated with a transition from a vibronically hot S_1 ($2^1A_g^-$) state to S_n. [10,24,25,31,46–48,60,69] This vibronically hot S_1 ($2^1A_g^-$) state is not evident in the global fits of any of the other LH2 complexes.

Global Analysis in the NIR Region. Because the spectral and temporal data in the NIR region were taken using a different detector from that used in the visible region, the global fitting analysis was done separately. Global fitting of the NIR data sets taken from the LH2 complex from *Rb. sphaeroides* G1C at 293 and 10 K are shown in Figure 8B,D. Four components were needed to obtain a satisfactory fit at both temperatures. The first EADS (black lines in Figure 8B,D) shows very strong positive peaks at 925, 1012, and 1134 nm at 293 K. At 10 K, the peaks appear at 920, 1012, 1134, and 1294 nm. This EADS component has a lifetime of 60 fs (293 K) and 110 fs (10 K), both of which are assigned to ESA from the S_2 ($1^1B_u^+$) state to higher singlet state. The longer wavelength bands disappear in going from the first to the second EADS (red lines in Figure 8B,D) which has a lifetime of 1.5 (293 K) and 1.4 ps (10 K). The strong positive band at 925 nm persists in both EADS. This amplitude has been assigned to the formation of a $Car^{\bullet+}$ of neurosporene.[8,75] The fact that it appears in both the first and the second EADS indicates that the $Car^{\bullet+}$ is formed from the S_2 ($1^1B_u^+$) state. The third EADS (green lines in Figure 8B,D) having a lifetime of 15 (293 K) and 5.9 ps (10 K) reveals that the amplitude of the $Car^{\bullet+}$ spectrum decays and shifts to shorter wavelength. Although the shift may be attributable to vibronic cooling of the radical signal, the drop in intensity is probably indicative of charge recombination. In the fourth, infinitely long (in this experimental time window) EADS (blue lines in Figure 8B,D) bands beyond 900 nm have completely decayed away, but the negative bands associated with the photobleaching and emission of the BChl B850 Q_Y transition persist as expected.

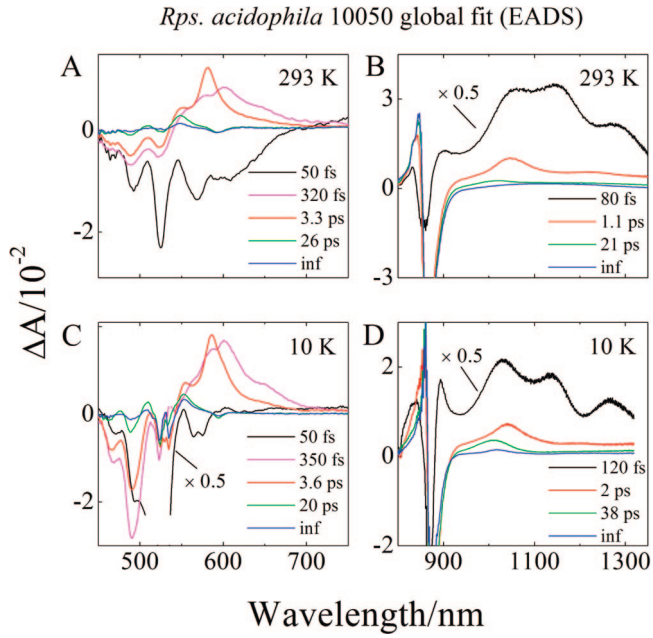

Figure 9. Evolution associated difference spectra (EADS) of LH2 from *Rps. acidophila* 10050.

The EADS components derived from global fits of the 293 and 10 K NIR data sets from the LH2 complexes from *Rb. sphaeroides* 2.4.1 (anaerobic), *Rb. sphaeroides* 2.4.1 (aerobic), and *Rps. acidophila* 10050 are shown in Supporting Information, Figures S4B,D and S5B,D, and Figure 9B,D, respectively. All the results are similar to those obtained from the analysis of the data from the LH2 complex from *Rb. sphaeroides* G1C described above with the following differences: (1) The peak positions appearing in the first EADS (black lines in Figures 8, 9, S4, S5, B and D) associated with the Car S_2 ($1^1B_u^+$) → S_n transition are red-shifted with increasing π-electron conjugated chain length of the Car; (2) The peak positions appearing in the second EADS (red lines in Figures 8 and 9 and Supporting Information Figures S4 and S5B,D) associated with the $Car^{\bullet+}$ are also red-shifted with increasing π-electron conjugated chain length of the Car, except for the peak in the EADS of the LH2 complex from *Rb. sphaeroides* 2.4.1 (aerobic). The values are 925 nm (293 and 10 K) for LH2 from *Rb. sphaeroides* G1C, 981 (293 K) and 972 nm (10 K) for LH2 from *Rb. sphaeroides* 2.4.1 (anaerobic), 960 (293 K) and 959 nm (10 K) for LH2 from *Rb. sphaeroides* 2.4.1 (aerobic), and 1045 (293 K) and 1042 nm (10 K) for LH2 from *Rps. acidophila* 10050.

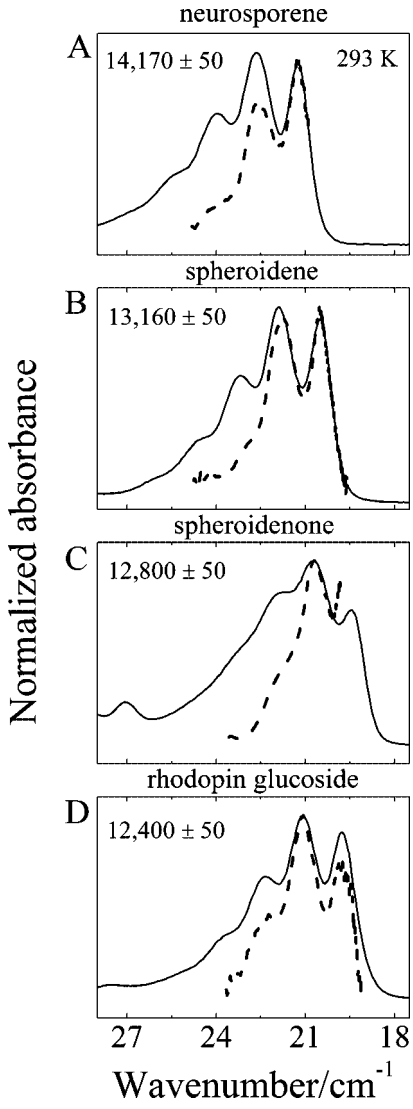

Figure 10. Overlay of the steady-state S_0 ($1^1A_g^-$) → S_2 ($1^1B_u^+$) absorption (solid line) and the S_1 ($2^1A_g^-$) → S_2 ($1^1B_u^+$) transient absorption (dashed line) shifted from the NIR region by the indicated amount of energy in cm^{-1} units. (A) neurosporene, (B) spheroidene, (C) spheroidenone, and (D) rhodopin glucoside. All spectra were taken at 293 K in acetone except spheroidenone, which was measured in hexane.

For all the NIR EADS profiles of the LH2 complexes, in going from the second (red lines in Figures 8 and 9 and Supporting Information, Figures S4 and S5B,D) to the third (green lines in Figures 8 and 9 and Supporting Information, Figures S4 and S5B,D) trace, the positive band assigned to the $Car^{\bullet+}$ shifts to shorter wavelength and decreases in intensity. This behavior is exemplified in the second and the third EADS in *Rps. acidophila* 10050 (red and green lines in Figures 9B,D). In most cases, narrowing of the $Car^{\bullet+}$ band accompanies the shifting. This observation and the fact that the lifetime of the second EADS component is on the order of 1 ps or less suggest that the effect is due to vibrational relaxation occurring in the D_0 state of the $Car^{\bullet+}$ accompanied by charge recombination.

S_1 ($2^1A_g^-$) State Energies of the Cars. The energies of the S_1 ($2^1A_g^-$) states of the Cars were determined to 50 cm^{-1} precision for the purified all-*trans* molecules in solution by measuring the S_1 ($2^1A_g^-$) → S_2 ($1^1B_u^+$) transient spectra in the NIR region and then shifting the spectra (dotted lines in Figure 10) to correspond to the S_0 ($1^1A_g^-$) → S_2 ($1^1B_u^+$) steady-state spectra (solid lines in Figure 10). The magnitude of the shift required to bring the spectra into agreement corresponds to the S_1 ($2^1A_g^-$) energy of the Car. These values are important for understanding the mechanism of EET from Car to BChl in the LH2 complexes, and are summarized in Table 1 along with the S_2 ($1^1B_u^+$) energies of the Cars and the S_1 and S_2 energies of the B800 and B850 BChls.

Discussion

Pathways of Carotenoid Excited-State Relaxation. Measurements by fluorescence excitation spectroscopy (Figure 5) reveal a precipitous drop in the Car-to-BChl energy transfer efficiency from ~90% for the LH2 complexes from *Rb. sphaeroides* G1C and 2.4.1 (anaerobic and aerobic) to ~53% for the LH2 complex from *Rps. acidophila* 10050. There are three possible reasons for this behavior: (1) The LH2 complexes from *Rb. sphaeroides* G1C and 2.4.1 (anaerobic and aerobic) possess a Car-to-BChl EET pathway unavailable to the LH2 complex from *Rps. acidophila* 10050; (2) The LH2 complex from *Rps. acidophila* 10050 possesses an alternate dissipative route of Car excitation not used by the other LH2 complexes; or (3) Structural differences exist between the LH2 complexes from *Rb. sphaeroides* G1C and 2.4.1 (anaerobic and aerobic) compared to the LH2 complex from *Rps. acidophila* 10050 which lead to different electronic couplings controlling EET.

There are several pathways for Car excited-state deactivation, and all the possibilities need to be considered to understand the mechanism of Car-to-BChl EET. The time constants for de-excitation of the Car excited states obtained from the global fitting analysis of the spectral and temporal data sets provide information on how the efficiency of Car-to-BChl EET is partitioned among the various routes. As mentioned in the introduction, the position of the $1^1B_u^-$ state, and its involvement in controlling the dynamics of excited states deactivation, are controversial issues. Therefore, in the initial analysis, a simplified model (Figure 2) was used based on the two undisputed pathways for the decay of the photoexcited S_2 ($1^1B_u^+$) state. These are internal conversion to S_1 ($2^1A_g^-$), and EET to the B800 and B850 BChl S_2 states (Figure 2). The total Car-to-BChl energy transfer efficiency can be expressed as

$$\phi_{ET} = \phi_{ET2} + \left(1 - \frac{\phi_{ET2}}{100}\right)\phi_{ET1} \qquad (1)$$

where ϕ_{ET1} and ϕ_{ET2} are the Car-to-BChl energy transfer efficiencies (in percent units) from the Car S_1 ($2^1A_g^-$) and S_2 ($1^1B_u^+$) states, respectively. The total EET efficiency for each LH2 complex has been determined by steady-state fluorescence excitation experiments (see Figure 5). The validity of this simplified model, illustrated graphically in Figure 2, can be tested by comparing the efficiencies obtained from the fluorescence excitation measurements, $\phi_{ET(flex)}$ with the values obtained from the dynamics of the S_1 ($2^1A_g^-$) and S_2 ($1^1B_u^+$) excited states, $\phi_{ET(dyn)}$. ϕ_{ET1} and ϕ_{ET2} can be deduced independently from the lifetimes of the S_1 ($2^1A_g^-$) and S_2 ($1^1B_u^+$) states in solution and in the LH2 complexes. The relevant expression is

$$\phi_{ETi} = \left(1 - \frac{\tau_{S_i}^{LH2}}{\tau_{S_i}^{SOLN}}\right) \times 100 \qquad i = 1, 2 \qquad (2)$$

where $\tau_{S_1}^{SOLN}$ and $\tau_{S_2}^{LH2}$ are the lifetimes of the excited singlet states in solution and in the LH2 complexes, respectively, and i indexes the state S_1 ($2^1A_g^-$) or S_2 ($1^1B_u^+$). Table 2 summarizes the efficiencies, ϕ_{ET}, ϕ_{ET1}, ϕ_{ET2}, lifetimes, $\tau_{S_1}^{SOLN}$,

TABLE 2: Efficiencies of Energy Transfer, ϕ_{ET1}, ϕ_{ET2}, $\phi_{ET(dyn)}$, $\phi_{ET(flex)}$, Energy Transfer Rate Constants, k_{ET1} and k_{ET1}, and Lifetimes, $\tau_{S_1}^{LH2}$, $\tau_{S_1}^{SOLN}$, $\tau_{S_2}^{LH2}$, $\tau_{S_2}^{SOLN}$ of the S_1 ($2^1A_g^-$) and S_2 ($1^1B_u^+$) Excited States of the Cars, Neurosporene, Spheroidene, Spheroidenone and Rhodopin Glucoside Obtained in Solution and in the LH2 Complexes at 293 and 10 K (Uncertainties Correspond to the Standard Deviation of a Mean of Measurements or a Range of Values Based on the Experimental Results)

LH2 complex (carotenoid)	T (K)	$\tau_{S_1}^{LH2}$ (ps)	$\tau_{S_1}^{SOLN}$ (ps)[a]	k_{ET1} (ps^{-1})	ϕ_{ET1} (%)[c]	$\tau_{S_1}^{LH2}$ (fs)[d]	$\tau_{S_1}^{SOLN}$ (fs)[b]	k_{ET2} (ps^{-1})	ϕ_{ET2} (%)[c]	$\phi_{ET(dyn)}$ (%)[e]	$\phi_{ET(flex)}$ (%)[f]
Rb. sphaeroides G1C (neurosporene)	293	1.2 ± 0.1	24 ± 1	0.8 ± 0.1	95 ± 1	70 ± 10	200 ± 20	9.3 ± 2.8	65 ± 7	98 ± 1	91 ± 5
	10	0.9 ± 0.1	34.8 ± 0.1	1.1 ± 0.1	97 ± 1	110 ± 10	140 ± 5	1.9 ± 1.0	21 ± 10	98 ± 1	91 ± 8
Rb. sphaeroides 2.4.1 anaerobic (spheroidene)	293	1.5 ± 0.1	7.9 ± 0.7	0.6 ± 0.1	82 ± 3	115 ± 15	230 ± 10	4.3 ± 1.5	48 ± 10	91 ± 2	93 ± 5
	10	1.5 ± 0.1	11.6 ± 0.1	0.6 ± 0.1	87 ± 2	130 ± 30	200 ± 5	2.7 ± 2.4	35 ± 17	92 ± 3	88 ± 5
Rb. sphaeroides 2.4.1 aerobic (spheroidenone)	293	0.8 ± 0.1	6.0 ± 0.1[g]	1.1 ± 0.2	87 ± 2	100 ± 10	180 ± 10[g]	4.4 ± 1.4	44 ± 9	93 ± 2	94 ± 5
	10	0.9 ± 0.1	6.0 ± 0.1[g]	0.9 ± 0.2	85 ± 2	120 ± 40	180 ± 10[g]	3.8 ± 3.4	32 ± 26	90 ± 5	92 ± 5
Rps. acidophila 10050 (rhodopin glucoside)	293	3.3 ± 0.2	4.3 ± 0.1	0.07 ± 0.03	23 ± 7	60 ± 10	160 ± 10[g]	10 ± 4	63 ± 10	71 ± 8	54 ± 5
	10	3.6 ± 0.1	5.9 ± 0.1	0.11 ± 0.01	39 ± 3	90 ± 40	150 ± 10	7.2 ± 6.6	38 ± 31	63 ± 22	52 ± 6

[a] Average values from Niedzwiedzki et al. [b] At 293 K in acetone and CS_2 and at 77 K in EPA (5/5/2, ether/isopentane/ethanol, v/v/v). [c] Calculated from eq 2 in the text. [d] Average S_2 state lifetimes obtained from global fitting of the transient spectra in the VIS and NIR regions. [e] Calculated from eq 1 in the text. [f] Determined from fluorescence excitation measurements (see Figure 5). [g] Obtained from global fitting of transient absorption data taken in acetone (rhodopin glucoside in NIR region) or in hexane (spheroidenone in the VIS and NIR regions) at 293 K.

$\tau_{S_1}^{LH2}$, $\tau_{S_2}^{SOLN}$, $\tau_{S_2}^{LH2}$, and rate constants, $k_{ET1} = 1/\tau_{S_2}^{LH2} - 1/\tau_{S_2}^{SOLN}$, and $k_{ET1} = 1/\tau_{S_2}^{LH2} - 1/\tau_{S_2}^{SOLN}$ derived from these data. One important result is the approximate order of magnitude lower value for the k_{ET1} rate constant for the LH2 complex from *Rps. acidophila* 10050 compared to the other complexes. This indicates that the pathway of EET involving the S_1 ($2^1A_g^-$) state of rhodopin glucoside is substantially inhibited. The values of the rate constants, k_{ET2}, however, remain relatively constant for the four complexes suggesting that this pathway is uniformly active. For the LH2 complexes from *Rb. sphaeroides* G1C and 2.4.1 (anaerobic and aerobic), the Car-to-BChl energy transfer efficiencies obtained from steady-state fluorescence excitation measurements ($\phi_{ET(flex)}$ in Table 2) are in reasonable agreement with those deduced from the dynamics of the excited singlet states determined from eqs 1 and 2 ($\phi_{ET(dyn)}$ in Table 2). This supports the validity of the simplified model presented in Figure 2 for these systems. In the case of the LH2 complex from *Rps. acidophila* 10050 the model significantly overestimates the total EET efficiency. Clearly, in all cases the simplified model can only be considered qualitatively correct because the transient absorption data taken in the visible region indicate some portion of the excited-state population forms the S* state, and the spectra in the NIR region reveal the formation of Car radical cations ($Car^{\bullet+}$). Thus, it is important to evaluate the yields of these species and ask whether they have any affect on controlling EET in the LH2 complexes.

Carotenoid Radical Cation Formation. Transient optical absorption signals in the 900−1100 nm NIR region with decay times in the range 5.9−38 ps are attributable to the formation of Car radical cations, $Car^{\bullet+}$. These signals are formed from the Car S_2 ($1^1B_u^+$) state very rapidly, and then undergo vibronic cooling prior to deactivation to the ground-state via charge recombination. Because the extinction coefficient of the $D_0 \rightarrow D_2$ transition of a $Car^{\bullet+}$ is very similar to that of the S_0 ($1^1A_g^-$) $\rightarrow$ S_2 ($1^1B_u^+$) transition of a neutral Car,[74] the relative yield of radical cations that persist after vibrational cooling may be obtained from a ratio of the third EADS amplitude in the NIR (green lines in Figure 8 and 9 and Supporting Information, Figures S4 and S5B,D) to that of the initial Car ground-state bleaching in the visible region (black lines in Figures 6 and 7 and Supporting Information, Figures S1 and S2A,C). The yield is given by

TABLE 3: Relative Yields of Carotenoid Radical Cations[a]

LH2 complex (carotenoid)	T (K)	$\phi_{Car^{\bullet+}}$ (%)
Rb. sphaeroides G1C(neurosporene)	293	11 ± 1
	10	5.0 ± 0.6
Rb. sphaeroides 2.4.1 anaerobic(spheroidene)	293	7.2 ± 0.7
	10	1.7 ± 0.2
Rb. sphaeroides 2.4.1 aerobic(spheroidenone)	293	11 ± 0.7
	10	3.3 ± 0.3
Rps. acidophila 10050(rhodopin glucoside)	293	12 ± 1
	10	2.8 ± 0.2

[a] The values were computed from a ratio of the amplitudes of the bands associated with $Car^{\bullet+}$ formation and Car ground state bleaching as described in the text.

$$\phi_{Car^{\bullet+}} = \frac{A_{Car^{\bullet+}}}{A_{Car}} \times 100 \quad (3)$$

where $A_{Car^{\bullet+}}$ is the amplitude of the EADS component in the NIR, and A_{Car} is the amplitude associated with Car ground-state bleaching in the visible region. Using these values in eq 3, the yields of $Car^{\bullet+}$ formation for the different LH2 complexes were found to span a range from 7.2 to 12% at room temperature and from 1.7 to 5.0% at 10 K (Table 3). It is important to note that the yields given in Table 3 are those of the longest-lived Car radicals. The drop in amplitude in going from the second (red lines in Figures 8 and 9 and Supporting Information, Figures S4 and S5B,D) to the third (green lines in Figures 8 and 9 and Supporting Information, Figures S4, S5B,D) EADS are highly suggestive of rapid charge recombination of a population of the radicals. Also, although these yields are significantly lower at 10 K compared to room temperature, they do not show any obvious trend with conjugation length of the Car.

As previously mentioned, population transfer from S_2 ($1^1B_u^+$) to the S* state is also a pathway of Car excited-state deactivation. The inclusion of this pathway in the mechanism of Car excited-state decay complicates the kinetic model and renders the simple algebraic formalisms presented above inadequate for a comprehensive treatment of EET in LH2 complexes. For this reason, a target model-based analysis of the spectral and time-resolved data sets was employed.

Target Model Analysis. The models used for the target analysis are shown in Figure 11. In the interest of brevity, the analysis will deal only with the transient absorption data from

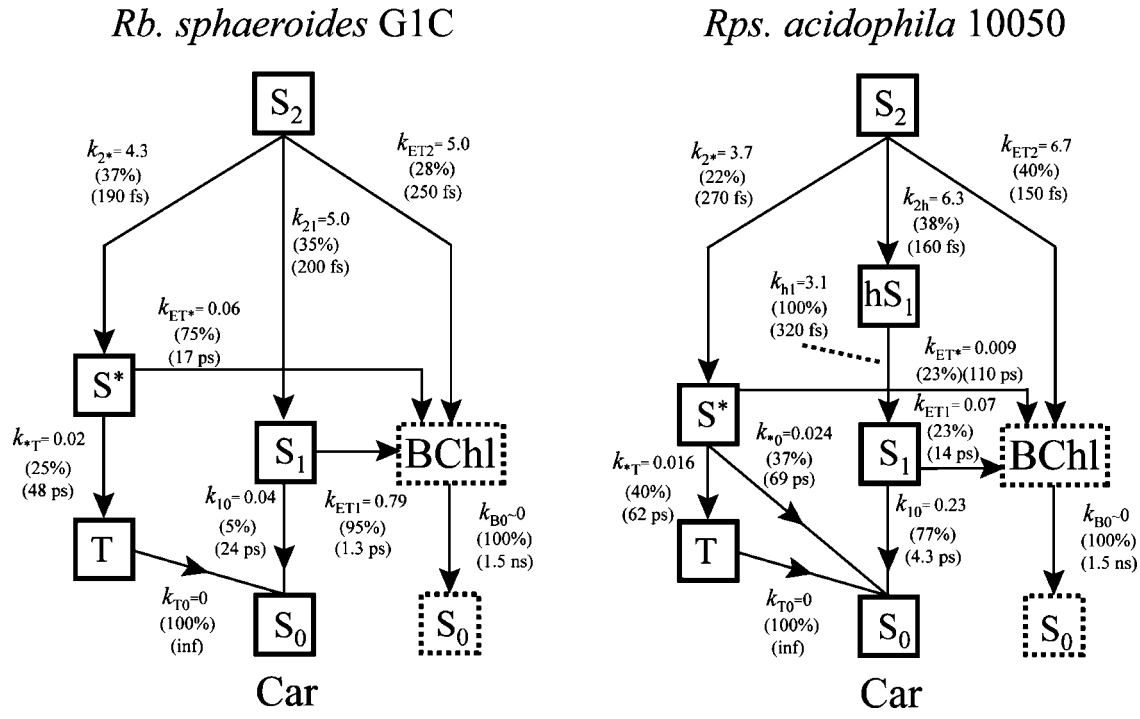

Figure 11. Energy flow pathways of LH2 complexes applied in the target analysis. hS_1 corresponds to a vibronically excited S_1 ($2^1A_g^-$) state of the Car. This intermediate is only evident in the transient absorption spectra and fitted lineshapes from the LH2 complex of *Rps. acidophila* 10050.

the LH2 complexes from *Rb. sphaeroides* G1C and *Rps. acidophila* 10050 taken in the visible region at 293 K. These may be considered limiting cases for the effect of π-electron conjugation length of the carotenoid in controlling Car-to-BChl EET. For the LH2 complex from *Rps. acidophila* 10050, a hot S_1 ($1^1A_g^-$) state was added to the model based on experimental observations described above. Radical cation formation was not included in the models because the transient absorption data in the visible region do not contain spectroscopic features attributable to them. Similar target models have been used previously to interpret transient absorption data taken at room temperature from the LH2 complexes from *Rb. sphaeroides* 2.4.1 and *Rps. acidophila* 10050.[10,31,44] In those publications, the kinetic parameters and branching yields for the deactivation pathways were treated as freely varying parameters. Here we set the branching yields for the decay of the various excited states *a priori* from a consideration of the extent of ground-state bleaching and recovery measured in different time domains. The branching yields were then used in conjunction with the effective lifetimes of the kinetic components obtained from the EADS global fitting analysis to converge on an acceptable fit to data. Species associated decay spectra (SADS) were obtained from the target models and examined for reasonableness in spectral line shape and position. If they were deemed acceptable, the rate constants for the various decay pathways were then used to compute $\phi_{ET(dyn)}$ values and fine-adjusted as needed to achieve good agreement with the $\phi_{ET(flex)}$ values.

LH2 Complex from Rb. Sphaeroides G1C. The branching yields for the decay of the S_2 ($1^1B_u^+$) state of neurosporene were determined as follows: The lifetime of the S_2 ($1^1B_u^+$) state of neurosporene in the LH2 complex at 293 K was found to be 70 fs $= 1/(k_{2*} + k_{ET2} + k_{21})$. The lifetime of the S_2 ($1^1B_u^+$) state of neurosporene in solution is 200 fs $= 1/k_{21}$. Therefore, the percent of S_2 ($1^1B_u^+$) population that decays to S_1 ($2^1A_g^-$) in the LH2 complex is $[k_{21}/(k_{2*} + k_{ET2} + k_{21})] \times 100 = (70/200) \times 100 = 35\%$. The remaining 65% either populates S* or is transferred to BChl. The fraction of this amount that populates S* can be obtained from a consideration of the transient absorption data in the region of the carotenoid ground-state bleaching. The ratio of the ground-state bleaching measured after energy transfer to BChl has been completed (at ~5 ps delay) to the initial ground-state bleaching measured just after the laser pulse (at ~50 fs delay) is 26% and is an approximation to the percent yield of S* formation. This is only an approximation, because at this time S* has already partially decayed away. Comparing the amplitude of the pure S* → S_n spectrum (at ~5 ps delay) with that of the "blue shoulder" on the S_1 ($2^1A_g^-$) → S_n transition (at ~200 fs delay) provides a scaling factor that account for the extent of S* decay at ~5 ps. After applying this scaling factor, the initial (and maximum) yield of S* formed from S_2 ($1^1B_u^+$) was found to be 37%. This also means that the portion of the initial S_2 ($1^1B_u^+$) population that is transferred to BChl is $100 - 37 - 35 = 28\%$. The same procedure can be used to obtain the extent of branching of population from S* to the Car triplet state. The transient absorption associated with the Car triplet state has a constant amplitude due to its essentially infinite lifetime in this experiment. The ratio of the S_0 ($1^1A_g^-$) → S_2 ($1^1B_u^+$) bleaching of the transient absorption spectrum taken after a few hundred picoseconds (when all other transitions have decayed away) to the S_0 ($1^1A_g^-$) → S_2 ($1^1B_u^+$) bleaching associated with the S*→S_n transition only (see above) gives the yield of the triplet state formation from S* and was found to be 25%. The remaining 75% is the amount of S* population transferred to BChl. Without this contribution, the total Car-to-BChl EET efficiency would be significantly underestimated.

The S_1 ($1^1A_g^-$) state branching yields in the LH2 complex from *Rb. sphaeroides* G1C were found from the data in Table 2: 95% of S_1 ($2^1A_g^-$) population is transferred to BChl and 5% decays directly to the ground state. It is important to note that this is 95% of the 35% of S_2 ($1^1B_u^+$) population that decays to S_1 ($2^1A_g^-$). Taking all pathways into account, a total EET value

TABLE 4: Fitting Parameters Derived from the Target Analysis Fit to the Data at 293 K Using the Models Presented in Figure 11

	S_2	hot S_1	S_1	S*	T	BChl	$\phi_{ET(dyn)}$
			Rb. sphaeroides G1C LH2				
τ_{eff} (k_{eff})	70 fs (14.3)	na	1.2 ps (0.83)	12 ps (0.08)	(~0)	1.5 ns (~0)	
branch (yield) (τ) (k)	$S_2 \rightarrow S_1$ (35%) (200 fs) (5.0)		$S_1 \rightarrow S_0$ (5%) (24 ps) (0.04)	S*→T (25%) (48 ps) (0.02)			
	$S_2 \rightarrow$S* (37%) (190 fs) (5.3)		$S_1 \rightarrow$BChl (95%) (1.3 ps) (0.79)	S*→BChl (75%) (17 ps) (0.06)			
	$S_2 \rightarrow$BChl (28%) (250 fs) (4.0)						
EET (%)	28	0	33	28	0	na	89
			Rps. acidophila 10050 LH2				
τ_{eff} (k_{eff})	60 fs (16.7)	320 fs (6.3)	3.3 ps (0.3)	26 ps (0.039)	(~0)	1.5 ns (~0)	
branch (yield) (τ) (k)	$S_2 \rightarrow$hot S_1 (38%)(160 fs) (6.3)	$S_2 \rightarrow S_1$ (100%)	$S_1 \rightarrow S_0$ (77%) (4.3 ps) (0.23)	S*→T (40%) (62 ps) (0.016)			
	$S_2 \rightarrow$S* (22%) (270 fs) (3.7)		$S_1 \rightarrow$BChl (23%) (14 ps) (0.07)	S*→S_0 (37%) (69 ps) (0.014)			
	$S_2 \rightarrow$BChl (40%) (150 fs) (7.5)			S*→BChl (23%) (110 ps) (0.009)			
EET (%)	40	0	9	5	0	na	54

of 89% was obtained and is in excellent agreement with 91 ± 5% obtained from steady-state fluorescence excitation experiments (Figure 5). This model and the branching percentages are summarized in Figure 11 and in Table 4.

These branching yields were used as fixed parameters in the target analysis of the transient data sets from the LH2 complex from *Rb. sphaeroides* G1C. The resulting SADS are shown in Figure 12A. The goodness of fit was judged by the reasonableness of the spectral profiles and the requirement that the amplitude spectra of each species agree with the maxima in the signals obtained in the raw data. If it was found, e.g., after ~200 fs, that the SADS were significantly smaller or larger than the raw spectra, the fit was rejected. Comparing Figure 12A with Figure 6A one can see the amplitudes of the lineshapes agree very well. The dynamics of the SADS global fits reveal a 70 fs lifetime component associated with stimulated emission from S_2 ($1^1B_u^+$), a 1.2 ps lifetime component associated with the S_1 ($2^1A_g^-$) lifetime, and a 12 ps decay constant for S*. An infinitely long SADS component combines transient absorption

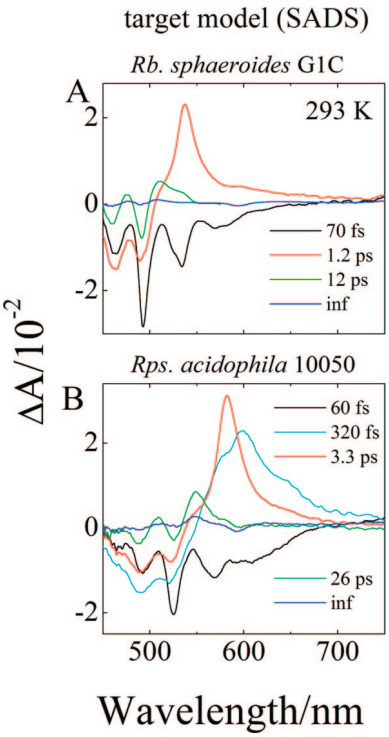

Figure 12. Species associated difference spectra (SADS) of LH2 from *Rb. sphaeroides* G1C and *Rps. acidophila* 10050 obtained using global fitting with the target models presented in Figure 11.

from the carotenoid triplet state and bleaching of the Q_x band of BChl which cannot be time-resolved in the temporal window of the experiment. The SADS spectral profiles are very reasonable and attest to the acceptability of the model.

LH2 Complex from Rps. Acidophila 10050. The target analysis for the data set from the LH2 complex from *Rps. acidophila* 10050 followed the same line of reasoning as described above for *Rb. sphaeroides* G1C. The branching yields for the decay of the S_2 ($1^1B_u^+$) state of rhodopin glucoside were determined from the lifetime of the S_2 ($1^1B_u^+$) state in the LH2 complex at 293 K which is 60 fs = $1/(k_{2*} + k_{ET2} + k_{2h})$. The lifetime of the S_2 ($1^1B_u^+$) state of rhodopin glucoside in solution is 160 fs = $1/k_{2h}$. Thus, the percent of S_2 ($1^1B_u^+$) population that decays to the vibronically hot S_1 ($2^1A_g^-$) state and ultimately to the relaxed S_1 ($2^1A_g^-$) state in the LH2 complex is $[k_{2h}/(k_{2*} + k_{ET2} + k_{21})] \times 100 = (60/160) \times 100 = 38\%$. The remaining 62% either populates S* or is transferred to BChl. The yield of the S* formation from S_2 ($1^1B_u^+$) was found in a manner similar to that used for the LH2 from *Rb. sphaeroides* G1C (see above). The ratio of the ground-state bleaching measured after energy transfer to BChl has been completed (at ~12 ps delay) compared to the initial ground-state bleaching measured just after the laser pulse (at ~50 fs delay) is 0.15. The S* yield was found from this ratio to be 22% after applying a scaling factor as described above for the G1C complex. On the basis of previous work[10,31] and the similarity of the lifetime of the hot S_1 ($2^1A_g^-$) state component in the LH2 complex compared to that measured in solution,[25] no branching of this state was assumed. This leads to a $(100 - 22 - 38) = 40\%$ yield of EET from the S_2 ($1^1B_u^+$) state to BChl. Also, using the procedure described above, the yield of triplet state formation branching from S* was found to be 40%. Of the remaining 60% of the S* population, 23% was required to account for EET to BChl, otherwise the total EET efficiency derived from the model would be underestimated compared to the value measured from fluorescence excitation experiments. The final 37% of the S* population was assumed to decay directly to the ground state. The branching yields from the S_1 ($2^1A_g^-$) state were determined from the kinetics presented in Table 2. It was found that 23% of the S_1 ($2^1A_g^-$) population is transferred to BChl and 77% decays directly to the ground state. The branching percentages are summarized in Figure 11 and in Table 4.

As described above for *Rb. sphaeroides* G1C these branching yields may now be used in a target analysis of the transient data sets from the LH2 from *Rps. acidophila* 10050. The resulting SADS are shown in Figure 12B. The dynamics of the SADS global fits reveal a 60 fs lifetime component associated with stimulated emission from S_2 ($1^1B_u^+$), a 320 fs component

associated with a vibronically hot S_1 ($2^1A_g^-$) → S_n transition, a 3.3 ps lifetime component associated with the decay of the S_1 ($2^1A_g^-$) state, and a 26 ps decay constant for S*. An infinitely long SADS component is attributable to transient absorption from the Car triplet state and bleaching of the Q_x band of BChl which cannot be temporally resolved in the time window of the experiment. As concluded above based on the target analysis of the data from the LH2 complex from *Rb. sphaeroides* G1C, these SADS profiles are also very reasonable and provide a compelling case for the correctness of the model.

Effect of Energy Levels on EET Efficiency. One explanation for the lower EET efficiency for the LH2 complex from *Rps. acidophila* 10050 is that the S_1 ($2^1A_g^-$) energy of rhodopin glucoside falls below that of the BChl S_1 state thereby reducing its ability to act as an energy donor to BChl. The actual values for the S_1 ($2^1A_g^-$) energies determined here for neurosporene, spheroidene, spheroidenone, and rhodopin glucoside are 14 170 ± 50, 13 160 ± 50, 12 800 ± 50, and 12 400 ± 50 cm^{-1}, respectively (Figure 10 and Table 1). All of these Car S_1 ($2^1A_g^-$) energies are above the S_1 energy of the B850 BChl which ranges from 11 510 to 11 810 cm^{-1}. Moreover, all of the Car S_1 ($2^1A_g^-$) energies *except* for that of rhodopin glucoside, are above the S_1 energy of the B800 BChl which ranges from 12 470 to 12 530 cm^{-1}. The fact that the S_1 ($2^1A_g^-$) energy of rhodopin glucoside lies below the S_1 state of the B800 BChl strongly suggests this is a factor responsible for the lower efficiency of Car-to-BChl EET in the LH2 complex from *Rps. acidophila* 10050 compared to the other complexes.

A more rigorous quantitative assessment of this issue is obtained by considering the spectral overlap between the Car donor emission and the acceptor BChl absorption given in the expression for the rate constant for energy transfer between weakly coupled donor−acceptor pairs.[79]

$$k_{ET} = \frac{1}{c\hbar}|T|^2 J \tag{4}$$

where T is the electronic coupling term, and J is the spectral overlap given by

$$J = \frac{\int_0^\infty F_d(\nu)\varepsilon_a(\nu)d\nu}{\int_0^\infty F_d(\nu)d\nu \int_0^\infty \varepsilon_a(\nu)d\nu} \tag{5}$$

$F_d(\nu)$ is the fluorescence spectrum of the donor, and $\varepsilon_a(\nu)$ corresponds to the absorption of the acceptor on a frequency (ν) scale. With an appropriate expression for T, eq 4 may be applied to any type of EET between weakly coupled donor−acceptor pairs.[80] Figure 13A,B shows the spectral overlap between the LH2 Q_X and Q_Y BChl absorption bands from *Rb. sphaeroides* 2.4.1 and the fluorescence traces obtained from 3,4,5,6-tetrahydrospheroidene, a spheroidene derivative having $N = 8$. This molecule exhibits fluorescence from both the S_1 ($2^1A_g^-$) and S_2 ($1^1B_u^+$) states, and its lineshapes are highly representative of those from open-chain Cars.[81] The fluorescence spectra were shifted to correspond to the spectral origins of the S_1 ($2^1A_g^-$) → S_0 ($1^1A_g^-$) and S_2 ($1^1B_u^+$) → S_0 ($1^1A_g^-$) transitions of the Cars in the LH2 complexes (Table 1). Because the S_0 ($1^1A_g^-$) → S_1 ($2^1A_g^-$) transition is symmetry forbidden, its transition dipole moment is very small, and the spectral origins of any transitions associated with the S_1 ($2^1A_g^-$) state measured in solution are expected to be very close to those of the Cars incorporated in the LH2 complexes. Also, the reported values show essentially no dependence on temperature.[56] Figure

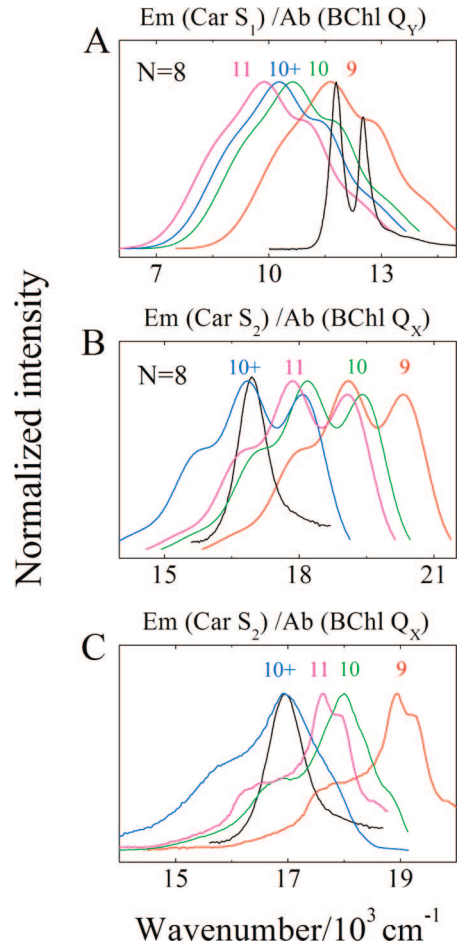

Figure 13. (A) Spectral overlap between the absorption of the LH2 Q_X and Q_Y BChl bands from *Rb. sphaeroides* 2.4.1 and a typical S_1 ($2^1A_g^-$) fluorescence trace taken from 3,4,5,6-tetrahydrospheroidene ($N = 8$) in petroleum ether shifted to correspond to the spectral origins of the S_1 ($2^1A_g^-$) → S_0 ($1^1A_g^-$) transition of neurosporene ($N = 9$), spheroidene ($N = 10$), spheroidenone ($N = 10+$), and rhodopin glucoside ($N = 11$). The S_1 ($2^1A_g^-$) energies for the Cars were determined from measurements of the S_1 ($2^1A_g^-$) → S_2 ($1^1B_u^+$) NIR transition energies (Figure 10). (B) Overlap between the absorption spectrum of the LH2 Q_X BChl band and a typical S_2 ($1^1B_u^+$) fluorescence trace taken from 3,4,5,6-tetrahydrospheroidene ($N = 8$) in petroleum ether shifted to correspond to the spectral origins of the S_2 ($1^1B_u^+$) → S_0 ($1^1A_g^-$) transition of the Cars in LH2 complexes. (C) Overlap between the absorption spectrum of the LH2 Q_X BChl band and the S_2 ($1^1B_u^+$) fluorescence taken from neurosporene, spheroidene, spheroidenone, and rhodopin glucoside in *n*-hexane shifted to correspond to the spectral origins of the S_2 ($1^1B_u^+$) → S_0 ($1^1A_g^-$) transition of the Cars in LH2 complexes.

13C shows the spectral overlap between the absorption of the LH2 Q_X BChl band and the S_2 ($1^1B_u^+$) fluorescence spectra of neurosporene, spheroidene, spheroidenone, and rhodopin glucoside taken in *n*-hexane, but shifted to correspond to the wavelength positions expected in the LH2 complexes. The numerical values for the spectral overlap were determined according to eq 5 and are summarized in Table 5. The spectral overlap between the S_1 ($2^1A_g^-$) → S_0 ($1^1A_g^-$) fluorescence and the B850 Q_Y BChl absorption band decreases gradually by an approximate factor of 2 (from 2.8 to 1.7), and the spectral overlap between the S_1 ($2^1A_g^-$) → S_0 ($1^1A_g^-$) fluorescence and the B800 Q_Y BChl absorption band decreases by a factor of approximately three (from 2.2 to 0.7) in going from $N = 9$ to 11. This indicates that EET from the Car S_1 ($2^1A_g^-$) state to the BChl S_1 state becomes less favorable as the conjugation length of the Car increases. A similar conclusion was reached

TABLE 5: Spectral Overlap of the LH2 Q_X and Q_Y Absorption Bands from *Rb. sphaeroides* 2.4.1 with Representative S_1 ($2^1A_g^-$) → S_0 ($1^1A_g^-$) and S_2 ($1^1B_u^+$) → S_0 ($1^1A_g^-$) Fluorescence Spectra of the Cars at 293 K[a]

	Car (S_1 → S_0) and BChl *a* (Q_Y)		Car (S_2 → S_0) and BChl[a] (Q_X)	
carotenoid	B800	B850	from Figure 13B	from Figure 13C
neurosporene	2.0	2.8	0.94	1.6
spheroidene	1.1	2.2	2.0	2.8
spheroidenone	0.78	1.8	2.9	2.5
rhodopin glucoside	0.56	1.3	2.3	3.1

[a] The S_1 ($2^1A_g^-$) energies were determined by the S_1 ($2^1A_g^-$) → S_2 ($1^1B_u^+$) transition from NIR transient absorption measurements.

by Kodis et al.[82] in an ultrafast study on synthetic carotenoid-phthalocyanine triads containing carotenoids with nine and ten conjugated double bonds. However, spectral overlap cannot account entirely for the sharp drop in efficiency because the S_1 → BChl energy transfer rate constant, k_{ET1}, deduced from the target analysis (Figure 11) decreases by a larger amount. Therefore, changes in electronic coupling among pigments must also be important. Interestingly, the spectral overlap between the S_2 ($1^1B_u^+$) → S_0 ($1^1A_g^-$) fluorescence and the Q_X BChl absorption, whether derived from the S_2 ($1^1B_u^+$) fluorescence of 3,4,5,6-tetrahydrospheroidene (Figure 13B) or from the fluorescence traces of the Cars themselves (Figure 13C), is approximately a factor of 2 times larger in going from the LH2 complex containing neurosporene ($N = 9$) to the complex containing rhodopin glucoside ($N = 11$). (See Table 4.) This indicates that the probability of EET from the Car S_2 ($1^1B_u^+$) state to the S_2 state of BChl becomes slightly enhanced as the extent of π-electron conjugation of the Car increases.

These data indicate that the path of EET from the S_1 ($2^1A_g^-$) state of the Car to BChl, especially that involving the B800 BChl, is significantly less available to rhodopin glucoside in the LH2 complex from *Rps. acidophila* 10050 compared the Cars in the other complexes. This fact coupled with the faster intrinsic S_1 ($2^1A_g^-$) state lifetime of the Car is the reason for the lower EET efficiency of this complex compared to the others. This notion is consistent with the fact that removal of the B800 BChl via treatment with the detergent, lauryl dodecyl sulfate (LDS), results in a significant drop in the efficiency of S_1-mediated energy transfer from >90 to ~70% in the LH2 complex from *Rb. sphaeroides* 2.4.1 containing spheroidene.[83] This conclusion is further supported by fluorescence excitation experiments on samples of the B850 (LH2) complex from the carotenoidless mutant *Rb. sphaeroides* R-26.1 reconstituted with spheroidene but naturally lacking the B800 BChl.[12] This preparation showed only a 30% S_1-mediated Car-to-B850 EET efficiency, consistent with the need for the Car S_1 ($2^1A_g^-$)-to-B800 pathway to achieve greater than 90% EET efficiency.[12]

The slight increase in spectral overlap of the Car S_2 ($1^1B_u^+$) emission band with the Q_X band of BChl with increasing π-electron chain length of the Car may be an example of nature making the best of a bad situation where the loss of energy transfer efficiency from the S_1 ($2^1A_g^-$) state of longer Cars is compensated for by maintaining a reasonable level of EET efficiency to BChl from the S_2 ($1^1B_u^+$) state. However, this is insufficient compensation for the loss of the B800 pathway of EET which is clearly necessary for a very high efficiency of EET from Car to BChl in LH2 complexes from photosynthetic bacteria.

Conclusions

Ultrafast time-resolved optical experiments coupled with global fitting of the spectral and temporal data sets have revealed the dynamics of the pathways of de-excitation of photoexcited carotenoid excited states and EET to BChl in the LH2 complexes from different strains of photosynthetic bacteria. For the LH2 complex from *Rb. sphaeroides* G1C containing neurosporene ($N = 9$), three routes of EET to BChl are active at 293K: S_2 ($1^1B_u^+$), S_1 ($2^1A_g^-$), and S*, and these contribute nearly equally (28%, $0.35 \times 0.95 \times 100\% = 33\%$, and $0.37 \times 0.75 \times 100\% = 28\%$, respectively) to the overall ~90% EET efficiency typical of complexes having carotenoids with $N < 11$. The dominant EET route for rhodopin glucoside ($N = 11$) in the LH2 complex from *Rps. acidophila* 10050 is via the S_2 ($1^1B_u^+$) state (40%), and this is almost twice as large as found for the *Rb. sphaeroides* G1C complex (28%). This conclusion is in agreement with the amount of spectral overlap of the Car S_2 ($1^1B_u^+$) emission with the BChl Q_X absorption which increases by a factor of ~2 in going from neurosporene ($N = 9$) to rhodopin glucoside ($N = 11$) (Table 5). The contribution of the S* state to the overall efficiency of EET in *Rps. acidophila* 10050 is $0.22 \times 0.23 \times 100\% = 5\%$ and smaller than that for *Rb. sphaeroides* G1C (28%). The data further reveal that the contribution to the efficiency of EET from the S_1 ($2^1A_g^-$) route for *Rb. sphaeroides* G1C (33%) and the other LH2 complexes having carotenoids with $N < 11$ is significant. For the LH2 complex from *Rps. acidophila* 10050 containing rhodopin glucoside, the S_1 ($2^1A_g^-$) route is much less probable ($0.38 \times 0.23 \times 100\% = 9\%$). Direct measurements of the S_1 ($2^1A_g^-$) energy levels of the Cars and the kinetic analysis done here indicate this is due primarily to the S_1 ($2^1A_g^-$) state of rhodopin glucoside being below that of the S_1 state of the B800 BChl.

Acknowledgment. The authors wish to thank Dr. Tomáš Polívka for several helpful discussions. This work is supported in the laboratory of H.A.F. by the National Institutes of Health (GM-30353). Support for the work carried out in the laboratory of R.J.C. is provided by the BBSRC. Partial support for components of the ultrafast laser spectrometer system was also provided by a grant to H.A.F. from the National Science Foundation (MCB-0314380).

Supporting Information Available: This material is available free of charge via the Internet at http://pubs.acs.org.

References and Notes

(1) Angerhofer, A.; Bornhauser, F.; Gall, A.; Cogdell, R. J. *Chem. Phys.* **1995**, *194*, 259.
(2) Frank, H. A.; Cogdell, R. J. *Photochem. Photobiol.* **1996**, *63*, 257.
(3) Akahane, J.; Rondonuwu, F. S.; Fiedor, L.; Watanabe, Y.; Koyama, Y. *Chem. Phys. Lett.* **2004**, *393*, 184.
(4) Cogdell, R. J. *Pure Appl. Chem.* **1985**, *57*, 723.
(5) McDermott, G.; Prince, S. M.; Freer, A. A.; Hawthornthwaite-Lawless, A. M.; Papiz, M. Z.; Cogdell, R. J.; Isaacs, N. W. *Nature (London)* **1995**, *374*, 517.
(6) Polívka, T.; Zigmantas, D.; Herek, J. L.; He, Z.; Pascher, T.; Pullerits, T.; Cogdell, R. J.; Frank, H. A.; Sundström, V. *J. Phys. Chem. B* **2002**, *106*, 11016.
(7) Papagiannakis, E.; Das, S. K.; Gall, A.; Stokkum, I. H. M.; Robert, B.; van Grondelle, R.; Frank, H. A.; Kennis, J. T. M. *J. Phys. Chem. B* **2003**, *107*, 5642.
(8) Polívka, T.; Pullerits, T.; Frank, H. A.; Cogdell, R. J.; Sundström, V. *J. Phys. Chem. B* **2004**, *108*, 15398.
(9) Polívka, T.; Sundström, V. *Chem. Rev.* **2004**, *104*, 2021.
(10) Papagiannakis, E.; van Stokkum, I. H.; Vengris, M.; Cogdell, R. J.; van Grondelle, R.; Larsen, D. S. *J. Phys. Chem. B* **2006**, *110*, 5727.
(11) Polli, D.; Cerullo, G.; Lanzani, G.; De Silvestri, S.; Hashimoto, H.; Cogdell, R. J. *Biophys. J.* **2006**, *90*, 2486.

(12) Polívka, T.; Niedzwiedzki, D.; Fuciman, M.; Sundström, V.; Frank, H. A. *J. Phys. Chem. B* **2007**, *111*, 7422.
(13) Papiz, M. Z.; Prince, S. M.; Howard, T.; Cogdell, R. J.; Isaacs, N. W. *J. Mol. Biol.* **2003**, *326*, 1523.
(14) Pariser, R. *J. Chem. Phys.* **1955**, *24*, 250.
(15) Callis, P. R.; Scott, T. W.; Albrecht, A. C. *J. Chem. Phys.* **1983**, *78*, 16.
(16) Birge, R. R. *Acc. Chem. Res.* **1986**, *19*, 138.
(17) Cosgrove, S. A.; Guite, M. A.; Burnell, T. B.; Christensen, R. L. *J. Phys. Chem.* **1990**, *94*, 8118.
(18) DeCoster, B.; Christensen, R. L.; Gebhard, R.; Lugtenburg, J.; Farhoosh, R.; Frank, H. A. *Biochim. Biophys. Acta* **1992**, *1102*, 107.
(19) Frank, H. A.; Farhoosh, R.; Decoster, B.; Christensen, R. L. *Molecular features that control the efficiency of carotenoid-to-chlorophyll energy transfer in photosynthesis*, Proceedings of the Ninth International Congress on Photosynthesis, Vol. 1, pp 125-8; Murata N., Ed., Nagoya, Japan, August 30-September 4, 1992; Kluwer Academic Publishers: Dordrect, Netherlands.
(20) Frank, H. A.; Farhoosh, R.; Aldema, M. L.; DeCoster, B.; Christensen, R. L.; Gebhard, R.; Lugtenburg, J. *Photochem. Photobiol.* **1993**, *57*, 49.
(21) Frank, H. A.; Christensen, R. L. Singlet energy transfer from carotenoids to bacteriochlorophylls. In *Anoxygenic Photosynthetic Bacteria*; Blankenship, R. E., Madigan, M. T., Bauer, C. E., Eds.; Kluwer Academic Publishers Dordrecht The Netherlands, 1995; Vol. 2; pp 373.
(22) Christensen, R. L. The electronic states of carotenoids In *The Photochemistry of Carotenoids*; Frank, H. A., Young, A. J., Britton, G., Cogdell, R. J. Eds.; Kluwer Academic Publishers: Dordrecht, 1999; Vol. 8, pp 137.
(23) Christensen, R. L.; Barney, E. A.; Broene, R. D.; Galinato, M. G. I.; Frank, H. A. *Arch. Biochem. Biophys.* **2004**, *430*, 30.
(24) Niedzwiedzki, D. M.; Sullivan, J. O.; Polivka, T.; Birge, R. R.; Frank, H. A. *J. Phys. Chem. B* **2006**, *110*, 22872.
(25) Niedzwiedzki, D.; Koscielecki, J. F.; Cong, H.; Sullivan, J. O.; Gibson, G. N.; Birge, R. R.; Frank, H. A. *J. Phys. Chem. B* **2007**, *111*, 5984.
(26) Christensen, R. L.; Galinato, M. G. I.; Chu, E. F.; Fujii, R.; Hashimoto, H.; Frank, H. A. *J. Am. Chem. Soc.* **2007**, *129*, 1769.
(27) Walla, P. J.; Linden, P. A.; Hsu, C.-P.; Scholes, G. D.; Fleming, G. R. *Proc. Natl. Acad. Sci. U.S.A.* **2000**, *97*, 10808.
(28) Macpherson, A. N.; Arellano, J. B.; Fraser, N. J.; Cogdell, R. J.; Gillbro, T. *Biophys. J.* **2001**, *80*, 923.
(29) Zhang, J. P.; Inaba, T.; Watanabe, Y.; Koyama, Y. *Chem. Phys. Lett.* **2001**, *340*, 484.
(30) Billstein, H. H.; Herek, J. L.; Garcia-Asua, G.; Hashoj, L.; Hunter, C. N.; Sundstrom, V. *Biochemistry* **2002**, *41*, 4127.
(31) Wohlleben, W.; Buckup, T.; Herek, J. L.; Cogdell, R. J.; Motzkus, M. *Biophys. J.* **2003**, *85*, 442.
(32) Rondonuwu, F. S.; Yokoyama, K.; Fujii, R.; Koyama, Y.; Cogdell, R. J.; Watanabe, Y. *Chem. Phys. Lett.* **2004**, *390*, 314.
(33) Tavan, P.; Schulten, K. *J. Chem. Phys.* **1979**, *70*, 5407.
(34) Tavan, P.; Schulten, K. *J. Chem. Phys.* **1986**, *85*, 6602.
(35) Tavan, P.; Schulten, K. *Phys. Rev. B: Condens. Matter* **1987**, *36*, 4337.
(36) Rondonuwu, F. S.; Watanabe, Y.; Fujii, R.; Koyama, Y. *Chem. Phys. Lett.* **2003**, *376*, 292.
(37) Fujii, R.; Inaba, T.; Watanabe, Y.; Koyama, Y.; Zhang, J. P. *Chem. Phys. Lett.* **2003**, *369*, 165.
(38) Koyama, Y.; Rondonuwu, F. S.; Fujii, R.; Watanabe, Y. *Biopolymers* **2004**, *74*, 2.
(39) Nishimura, K.; Rondonuwu, F. S.; Fujii, R.; Akahane, J.; Koyama, Y.; Kobayashi, T. *Chem. Phys. Lett.* **2004**, *392*, 68.
(40) Ikuta, M.; Yabushita, A.; Rondonuwu, F. S.; Akahane, J.; Koyama, Y.; Kobayashi, T. *Chem. Phys. Lett.* **2006**, *422*, 95.
(41) McCamant, D. W.; Kukura, P.; Mathies, R. A. *J. Phys. Chem. A.* **2003**, *107*, 8208.
(42) Kukura, P.; McCamant, D. W.; Mathies, R. A. *J. Phys. Chem. A* **2004**, *108*.
(43) Gradinaru, C. C.; Kennis, J. T. M.; Papagiannakis, E.; van Stokkum, I. H. M.; Cogdell, R. J.; Fleming, G. R.; Niederman, R. A.; van Grondelle, R. *Proc. Natl. Acad. Sci. U.S.A* **2001**, *98*, 2364.
(44) Papagiannakis, E.; Kennis, J. T. M.; van Stokkum, I. H. M.; Cogdell, R. J.; van Grondelle, R. *Proc. Nat. Acad. Sci. U.S.A* **2002**, *99*, 6017.
(45) Cerullo, G.; Polli, D.; Lanzani, G.; De Silvestri, S.; Hashimoto, H.; Cogdell, R. J. *Science* **2002**, *298*, 2395.
(46) Larsen, D. S.; Papagiannakis, E.; van Stokkum, I. H. M.; Vengris, M.; Kennis, J. T. M.; van Grondelle, R. *Chem. Phys. Lett.* **2003**, *381*, 733.
(47) Wohlleben, W.; Buckup, T.; Hashimoto, H.; Cogdell, R. J.; Herek, J. L.; Motzkus, M. *J. Phys. Chem. B* **2004**, *108*, 3320.
(48) Billsten, H. H.; Pan, J.; Sinha, S.; Pascher, T.; Sundström, V.; Polívka, T. *J. Phys. Chem. A* **2005**, *109*, 6852.
(49) Fujii, R.; Onaka, K.; Kuki, M.; Koyama, Y.; Watanabe, Y. *Chem. Phys. Lett.* **1998**, *288*, 847.
(50) Bautista, J. A.; Hiller, R. G.; Sharples, F. P.; Gosztola, D.; Wasielewski, M.; Frank, H. A. *J. Phys. Chem. A* **1999**, *103*, 2267.
(51) Frank, H. A.; Bautista, J. A.; Josue, J. S.; Young, A. J. *Biochemistry* **2000**, *39*, 2831.
(52) Zigmantas, D.; Polivka, T.; Hiller, R. G.; Yartsev, A.; Sundström, V. *J. Phys. Chem. A* **2001**, *105*, 10296.
(53) Fujii, R.; Ishikawa, T.; Koyama, Y.; Taguchi, M.; Isobe, Y.; Nagae, H.; Watanabe, Y. *J. Phys. Chem. A* **2001**, *105*, 5348.
(54) Josue, J. S.; Frank, H. A. *J. Phys. Chem. A* **2002**, *106*, 4815.
(55) Polívka, T.; Herek, J. L.; Zigmantas, D.; Akerlund, H. E.; Sundström, V. *Proc. Nat. Acad. Sci. U.S.A.* **1999**, *96*, 4914.
(56) Polívka, T.; Zigmantas, D.; Frank, H. A.; Bautista, J. A.; Herek, J. L.; Koyama, Y.; Fujii, R.; Sundström, V. *J. Phys. Chem. B* **2001**, *105*, 1072.
(57) Polívka, T.; Zigmantas, D.; Sundström, V.; Formaggio, E.; Cinque, G.; Bassi, R. *Biochemistry* **2002**, *41*, 439.
(58) Papagiannakis, E.; van Stokkum, I. H. M.; van Grondelle, R. *J. Phys. Chem. B* **2003**, *107*, 11216.
(59) Ilagan, R. P.; Christensen, R. L.; Chapp, T. W.; Gibson, G. N.; Pascher, T.; Polivka, T.; Frank, H. A. *J. Phys. Chem. A* **2005**, *109*, 3120.
(60) Pendon, Z. D.; Gibson, G. N.; van der Hoef, I.; Lugtenburg, J.; Frank, H. A. *J. Phys. Chem. B* **2005**, *109*, 21172.
(61) Meyer, B. *Low temperature spectroscopy*; American Elsevier: New York, 1971.
(62) Turro, N. J. *Modern Molecular Photochemistry*; University Science Books: Sausalito, CA, 1991.
(63) Frank, H. A.; Bautista, J. A.; Josue, J.; Pendon, Z.; Hiller, R. G.; Sharples, F. P.; Gosztola, D.; Wasielewski, M. R. *J. Phys. Chem. B* **2000**, *104*, 4569.
(64) Zigmantas, D.; Hiller, R. G.; Sharples, F. P.; Frank, H. A.; Sundstrom, V.; Polivka, T. *Phys. Chem. Chem. Phys.* **2004**, *6*, 3009.
(65) Koyama, Y.; Kuki, M.; Andersson, P. O.; Gillbro, T. *Photochem. Photobiol.* **1996**, *63*, 243.
(66) Gall, A.; Cogdell, R. J.; Robert, B. *Biochemistry* **2003**, *42*, 7252.
(67) Blankenship, R. E. Molecular Mechanisms of Photosynthesis; Blackwell Science: Oxford, 2002.
(68) Angerhofer, A.; Cogdell, R. J.; Hipkins, M. F. *Biochim. Biophys. Acta* **1986**, *848*, 333.
(69) Billsten, H. H.; Bhosale, P.; Yemelyanov, A.; Bernstein, P. S.; Polivka, T. *Photochem. Photobiol.* **2003**, *78*, 138.
(70) Herek, J. L.; Polivka, T.; Pullerits, T.; Fowler, G. J. S.; Hunter, C. N.; Sundstrom, V. *Biochem.* **1998**, *37*, 7057.
(71) Herek, J. L.; Wendling, M.; He, Z.; Polivka, T.; Garcia-Asua, G.; Cogdell, R. J.; Hunter, C. N.; van Grondelle, R.; Sundstrom, V.; Pullerits, T. *J. Chem. Phys. B* **2004**, *108*, 10398.
(72) Frank, H. A.; Cong, H.; Gibson,G. N.; Birge, R. R.; Niedzwiedzki, D. *Femtosecond time-resolved absorpton sepectroscopy of carotenoids*, 234th National Meeting of the American Chemical Society, Boston, MA, August 19-23, 2007; American Chemical Society: Washington, DC., 2007, PHYS-517.
(73) Jeevarajan, A. S.; Kispert, L. D.; Chumanov, G.; Zhou, C.; Cotton, T. M. *Chem. Phys. Lett.* **1996**, *259*, 515.
(74) Jeevarajan, J. A.; Wei, C. C.; Jeevarajan, A. S.; Kispert, L. D. *J. Phys. Chem.* **1996**, *100*, 5637.
(75) Galinato, M. G. I.; Niedzwiedzki, D.; Deal, C.; Birge, R. R.; Frank, H. A. *Photosynth. Res.* **2007**, *94*, 67.
(76) Cotton, T. M.; Van Duyne, R. P. *J. Am. Chem. Soc.* **1979**, *101*, 7605.
(77) Arlt, T.; Schmidt, S.; Kaiser, W.; Lauterwasser, C.; Meyer, M.; Scheer, H.; Zinth, W. *Proc. Natl. Acad. Sci. U.S.A.* **1993**, *90*, 11757.
(78) van Stokkum, I. H. M.; Larsen, D. S.; van Grondelle, R. *Biochim. Biophys. Acta* **2004**, *1657*, 82.
(79) Scholes, G. D.; Harcourt, R. D.; Fleming, G. R. *J. Chem. Phys. B* **1997**, *101*, 7302.
(80) Kasha, M. *Radiat. Res.* **1963**, *20*, 55.
(81) Desamero, R. Z. B.; Chynwat, V.; van der Hoef, I.; Jansen, F. J.; Lugtenburg, J.; Gosztola, D.; Wasielewski, M. R.; Cua, A.; Bocian, D. F.; Frank, H. A. *J. Phys. Chem.* **1998**, *102*, 8151.
(82) Kodis, G.; Herrero, C.; Palacios, R.; Mariño-Ochoa, E.; Gould, S.; de la Garza, L.; van Grondelle, R.; Gust, D.; Moore, T. A.; Moore, A. L.; Kennis, J. T. M. *J. Chem. Phys. B* **2004**, *108*, 414.
(83) Kramer, H. J. M.; van Grondelle, R.; Hunter, C. N.; Westerhuis, W. H. J.; Amesz, J. *Biochim. Biophys. Acta* **1984**, *765*, 156.
(84) Scheer, H. *Chlorophylls*; CRC Press: Boca Raton, 1991.

JP711946W